Internship Report
Natural convection flows inside differentially heated cavities

WRITTEN BY

PIM ADRIAAN BULLEE, BSC.
University of Twente

CONDUCTED AT

POLO
Research Laboratories for Emerging Technologies in Cooling and Thermophysics

UFSC
The Federal University of Santa Catarina

IN THE PERIOD

MARCH - JUNE 2014

UNDER SUPERVISION OF

PROF H.W.M. HOEIJMAKERS
University of Twente

PROF C.J. DESCHAMPS
Federal University of Santa Catarina

Abstract

A natural convection driven flow inside a differentially heated square cavity with aspect ratio 4 is studied. The cavity is filled with water and the Rayleigh number is determined to be 1.14×10^{10}. Measurement results from different heights obtained using Laser Doppler Velocimetry are presented. These results were used together with a literature study to make a statement regarding the results obtained by another researcher using the same cavity. Concluded is that because of a mistake made when setting up the measurement equipment, his results regarding the flow field near the cold wall are invalid. Apart from this, special care is taken in optimizing the measurement procedure by reviewing the number of measurements required to obtain a reliable average velocity value. Thereby the number of seeding particles inside the cavity that visualize the flow is optimized.

Nomenclature and abbreviations

C_p	specific heat capacity [kJ/(kg K)]
$f_{doppler}$	frequency related to the light scattered by the particles [1/s]
f_{shift}	change in frequency due to Bragg cell [1/s]
f_{signal}	frequency of the signal captured by the receiving optics [1/s]
g	acceleration due to gravity [m/s^2]
h	convective heat transfer coefficient [W/(m^2 K)]
H	height of the cavity 0.4 [m]
k	thermal conductivity [W/(m K)]
n	refractive index
p	static pressure [N/ms^2]
r_w	radius of laser beam waist [m]
t	thickness of the acrylic wall
T	temperature [K]
$\vec{u}$	velocity vector of the flow [m/s]
v_n	velocity normal to the lines of the interference pattern [m/s]

Dimensionless numbers

Nu_H	Nusselt number based on the cavity height; see Eq. 1.8
Pr	Prandtl number fluid property; see Eq. 1.7
Ra_H	Rayleigh number based on the cavity height; see Eq. 1.6

Greek symbols

α	thermal diffusivity $\alpha = k/\rho C_p$ [m^2/s]
β	volume expansion coefficient [1/K]
ΔT	temperature difference between the heated walls [K]
θ	angle of incident or transmitted light
μ	dynamic viscosity [kg/(m s)]
ν	kinematic viscosity [m^2/s]
ρ	density [kg/m^3]
$\bar{\bar{\tau}}$	viscous stress tensor [kg/ms^2]

Subscripts

a	air
c	cold wall
g	acrylic glass
h	hot wall
s	surface
w	water
∞	sufficiently far away (underscore ∞)

Abbreviations

AR	aspect ratio height versus width
CFD	computational fluid dynamics
DNS	direct numerical simulation
LDV	Laser Doppler velocimetry
LHS	left hand side of the equation
ODE	ordinary differential equation
PDE	partial differential equation
RHS	right hand side of the equation

Contents

Preface

This report is written during my three month internship in Florianópolis, Brazil. The goal of the research was to measure the flow field inside a rectangular cavity. This flow field is the result of natural convection inside the cavity, caused by a temperature difference between the two side walls. Together with me worked three bachelor students; Heitor, Domicio and Marcelo. They were of great help with my work and by the time I left, they were able to continue the measurements on their own.

The cavity we used had already been build and used before. However, it required maintenance. Rust was removed and some parts were painted again. The setup used to measure the temperature inside the cavity was redesigned and rebuild to be more durable. The measurement equipment had not been used since a long time as well. Therefore a lot of knowledge on the operation and maintenance of it had gone lost. Even the operating manuals and some parts of the setup were missing. Since no-one working at POLO had any experience in operating the measurement equipment, I spent my first two months a lot of time on finding out how to operate the equipment. Also a lot of time went into maintenance, testing, setting up to equipment and acquiring all the lost documents and parts. At some point even an external technician had to be of assistance. His conclusion was that the measurement equipment was in a state far from optimal. Nonetheless, in the last month I managed to perform some measurements and was able to finish my work.

To be of assistance to future researchers working in the lab, I decided in the first period of my internship to write an extensive operations manual. It is titled 'LDV Measurement Manual' and co-authored by Heitor Paes de Andrade. Since it features to much specific information and instructions, I decided against adding it to this report. It is handed in together with this report, but should be regarded as a separate piece of work, since it serves the sole intention of being of assistance to others working in the LDV lab at POLO.

This whole process made that I obtained a lot of knowledge on the measurement setup and equipment, which ultimately helped me in reaching the final conclusions of this report. It also resulted in that I had a lot of information and a lot of time to write it all down. The result is a substantial report and equally sized measurement manual. To compensate the reader who is more familiar with the subject, I wrote an extensive two page summary, which covers the most important parts of this report.

Extensive summary

The subject of study in this report is a natural convection driven flow inside a rectangular cavity. The cavity has dimensions 10 x 10 x 40 cm (width x depth x height) and is filled with water. The two side walls of the cavity are subjected to a temperature difference of ten degree Celsius. Near the hot wall, the water moves upwards due to the buoyancy effect. Near the cold wall the water moves downwards for the same reasons. The Rayleigh number for this setup is calculated to be 1.14×10^{10} using Equation 1.6. Based on the literature study presented in Section 2.3, it is concluded that for this Rayleigh number the flow inside the cavity is in the turbulent regime.

The natural convection driven flow inside a cavity models many practical engineering applications [1]. Thereby it also functions as a benchmark problem to validate numerical models [2]. Between 2010 and 2013, André Popinhak build and worked with the same setup as described in this report [3]. His results are shown in Figure A.1. The flow profiles near the cold wall are a bit different from the results obtained by other researchers. For instance Trias et al. performed numerical simulations at a Rayleigh number of 1.0×10^{10}. As can be seen in Figure 2.3, their results display symmetry between the hot and the cold wall side of the cavity in terms of the averaged velocity and temperature fields [2]. The results obtained by Popinhak do not show this symmetry. In his results, the flow profiles near the cold wall show a mere sinusoidal shape. This behaviour is explained by Popinhak as being caused by the fluid changing direction after encounter with the bottom wall. This results in a fluid intrusion moving upwards which disturbs the flow [3]. This particular phenomena is not present in the work by Trias et al.. Relevant experimental research has been conducted by Saury et al.. They worked with Rayleigh numbers between 4.0×10^{10} and 1.2×10^{11} [4]. Although their results do not display the perfect symmetry as was found numerically by Trias et al., a clear distinction exists with the results reported by Popinhak. The sinusoidal flow behaviour near the cold wall side of the cavity is not reported by Saury et al., nor is there mention given of an upwards travelling intrusion [4]. Since the near hot wall side results of Popinhak do show resemblance to the results obtained by both Trias et al. and Saury et al., there is reason enough to check the results from Popinhak by redoing his measurements.

The flow velocities in the cavity are measured using Laser Doppler Velocimetry (LDV) equipment. Polyamid particles with a diameter of 0.5 μm are added to the water in the

cavity to enhance the visibility of the flow. It turned out to be very important to add the correct amount of particles, since otherwise the measurement equipment was unable to detect the flow. In the operations manual of the measurement equipment is given that the optimal particle density is equal to the inverse of the measurement volume created by the LDV equipment [5]. The optimal total amount of particles to be added to the cavity was calculated to be ranging between 6×10^{-3} and 7×10^{-3} gram.

To create a flow profile, the flow velocity is measured at multiple points in the cavity. To determine the velocity at a specific point, the average velocity is calculated from multiple particles passing that point. To increase the efficiency of the measurements, the number of particles needed for an accurate average velocity is revised. In Figure 4.1 is shown that after 100 measurements, the average velocity is well within the boundaries of rounding. The data used to create one of the flow profiles is also shown to convergence in Figure 4.2.

The flow profiles at different heights in the cavity are plotted in Figure 4.3. The results near the hot wall side at half cavity height are missing due to time limitations. The flow profiles near the cold wall side of the cavity show, in contrary to the hot wall side, no resemblance to the results produced by Popinhak. The flow profiles near both the hot and the cold wall do show resemblance to the results from Trias et al. and Saury et al. as cited in [2] and [4].

The results presented in this report are produced identical to the way Popinhak produced his results. In order to gain further insight in what causes the difference in results, the settings files used by Popinhak to set up the measurement equipment are examined. These files were found on the computer used to perform measurements in the lab. Two of the variables that have to be set are related to the filter applied to the signal captured by the measurement equipment. Evaluation of the values chosen by Popinhak showed that the bandwidth of the filter that was chosen by Popinhak is to small. With his filter settings, only velocities ranging between -2.6 and 7.5 mm/s were allowed to pass. As can be seen in Figure 4.3, the velocities inside the cavity range between -8.5 and 8.5 mm/s. Therefore Popinhak was unable to correctly measure the velocities near the cold wall side.

What can not be explained is why a velocity of 8.5 mm/s shows up in the results from Popinhak in Figure A.1e and a velocity of -3 mm/s in Figure A.1i. Also, the cold wall results appear to be sinusoidal instead of a cut-off normal velocity profile. Since Popinhak gives in his master's thesis no information on the filter settings used, the reliability of his results is questionable.

It is therefore concluded, based on the wrongly chosen filter, the results presented in Figure 4.3 and the work of two different authors working with comparable setups, that the results and conclusions presented by Popinhak regarding the near cold wall velocities obtained using LDV measurements can be regarded as incorrect.

Chapter 1

Theoretical introduction

1.1 Introduction to heat transfer

All natural phenomena strive to reach an equilibrium or, a lowest state of energy. This can for instance be seen in a ball, which will always fall to the ground in order to minimize its gravitational energy. Or think of the water in a very quiet lake which is always levelled. There are never peaks and after a disturbance, the surface of the water will be flat again. The same goes for heat; nature always tries to redistribute heat to reach a constant equilibrium temperature. Placing a hot cup of coffee inside a room is metaphorically the same as throwing a little stone inside the quiet like. The disturbance, the local rise in temperature, will eventually be evened out and the cup of coffee will have the same temperature as its surroundings.

Conduction Conduction is the transport of heat on a molecular level. Particles with a higher energy transfer their energy in the form of heat to neighbouring particles with less energy. In gasses and liquids, this interaction is in the form of collisions and diffusion due to random motion of the particles. In solids, conduction is due to the vibrations of the atoms and the energy transport by free electrons. The amount of heat that can be transported by conduction is dependent of the material properties of the medium, but also on its dimensions and the temperature difference[6]. The amount of conductive heat transfer is defined using Equation 1.1

$$Q_{cond} = -kA\frac{\Delta T}{\Delta x} \tag{1.1}$$

In this equation k denotes the thermal conductivity [W/(m K)], which is a measure for the ability of a material to conduct heat. A denotes the area of the material normal to the direction of the conductive heat transfer, whereas Δx denotes the thickness of the material. By taking the limit of $\Delta x \to 0$ the equation is reduced to Fourier's law of heat conduction, which is given in Equation 1.2. It is named after Jean Baptiste Joseph Fourier, who first came up with this expression in 1822 [6].

$$Q_{cond} = -kA\frac{dT}{dx} \tag{1.2}$$

Radiation The best example of heat transfer by means of radiation is the energy from the sun that reaches the earth. This is by far the fastest way of energy transportation, since it travels at the speed of light. The energy transportation takes place in the form of electromagnetic waves which do not require the presence of any sort of medium; radiation from the sun travels through space which is a vacuum. Thermal radiation is emitted by objects due to their temperature and is therefore different from other types of radiation such as x-ray and microwaves. Thermal radiation can be felt by humans while x-ray and microwaves are senseless. Thermal radiation can for instance be observed when walking past a stone wall after a hot day. The wall has been heated by the sun all day and still maintains and radiates this heat during the cooler evening. The amount of heat transported by radiation is defined using the Stefan-Boltzmann law in Equation 1.3. It resulted from and was named after the combined works of Ludwig Boltzmann and Jožef Stefan by the end of the 19th century.

$$Q_{emit} = \sigma \omega A_s T_s^4 \tag{1.3}$$

The σ in Equation 1.3 denotes the Stefan-Boltzmann constant, equal to 5.67 $\times 10^{-8}$ [W/(m^2 K^4)]. Different types of materials display different emissivity behaviour. Therefore ϵ gives the material dependent emissivity varying between 0 and 1. Aluminium foil for instance has a very low emissivity with an ϵ value of 0.07, whilst black and white paint have values of 0.98 and 0.90 respectively. A theoretically perfect radiating so called 'black body' has an ϵ value of 1 [6]. The surface area and its temperature are denoted by A_s and T_s respectively.

Convection Apart from energy transfer due to the random motion of molecules (conduction), the motion of the fluid will also transport heat in the presence of a temperature difference. The motion of the fluid is determined by the stream velocity of the flow. So the faster the fluid flows, the larger is the amount of heat transfer by convection. An example of this is blowing over a hot cup of soup. When blowing harder the soup will cool down faster and by not blowing at all the soup will cool down more slowly. The process of convection is actually conduction with fluid motion [6]. Consider for instance a hot solid block of material, being cooled by an airflow. The first very thin layer of air which is in direct contact with the block will have no velocity. This is called the no-slip boundary condition. It is caused by the viscosity of the fluid causing the fluid to stick to the wall of the block. Due to this zero velocity, heat can only be transferred from the block to the adjacent layer of air by the mechanism of conduction. In layers of air further away from the block this energy is carried away by convection. The rate of convective heat transfer is linear with the temperature difference and can be expressed using Newton's law of cooling given in Equation 1.4.

$$Q_{conv} = hA_s(T_s - T_\infty) \tag{1.4}$$

In this equation h is the convective heat transfer coefficient [W/(m^2 K)]. It is not a fluid property, but depends on all variables influencing the convection. Of influence are for instance the surface geometry, the nature of fluid motion and its properties as well as

the fluid velocity. Therefore the convective heat transfer coefficient is to be determined experimentally [6]. The temperature sufficiently far away from the surface is denoted by the subscript ∞. Convection can be driven by for instance using a fan, called forced convection, but the type of convection observed in this research is natural convection. This means that the fluid motion is not influenced by an external source but is caused by the rising of warmer particles creating a flow.

It is important to understand that usually heat transfer is due to a combination of the mechanisms of convection, conduction and radiation. One of the mechanisms can be dominant over the others, which mostly depends on environmental conditions.

1.2 Mechanisms of natural convection

A local change in temperature of a fluid will almost always result in an instability, or at least a distributed temperature field inside the fluid. For instance when a fluid at rest is heated from below and cooled from above, a situation is created where the cooler, more dense fluid lies on top of the warmer less dense fluid. This is an unstable situation and at a certain moment the warmer and less dense fluid will move upwards to float on the cooler, more dense fluid. The cooler layer will move downwards where it is heated, to expand and move upwards again. This results in a circulating vertical flow due to the constant heating and cooling and associated expansion and contraction of the fluid. The driving force for this phenomena is buoyancy, the same principle on which the floatation of ships and hot air balloons is based. A body of a certain density submerged in a medium with a higher density will experience, due to buoyancy, a force directed upwards. The size of the force is related to the amount of volume of the body that is actually submerged, which is the same as the amount of fluid displaced. This is known as Archimedes' principle (Eureka!), and is displayed in mathematical form in Equation 1.5.

$$F_{buoyancy} = \rho_{fluid}\, g V_{displaced} \tag{1.5}$$

In this equation g is the acceleration due to gravity (9.8 m/s^2), ρ is the density [kg/m^3] and V is the volume [m^3] of the fluid displaced.

When a natural convection flow will start to develop is, apart from the temperature difference, also depended of the fluid viscosity and the thermal conduction rate. For fluids with a high thermal conduction coefficient, the differences in temperature, and thus the density, will be more evenly distributed. So, for these types of fluids, heat transportation due to conduction is dominant over heat transport due to convection. Viscous forces inside the fluid and where the fluid is in contact with another medium (for instance a wall over which the fluid flows) counteract the movement of the fluid. So, for fluids with high viscosity coefficients, the temperature differences (and thus the differences in density) need to be larger in order to start a buoyancy driven flow. This threshold was first expressed by Rayleigh in the early 20th century and will be discussed in more detail in Section 1.4.

1.3 Natural convection in a rectangular closed cavity

In the research covered in this report, natural convection flows are studied inside a rectangular cavity. The cavity has dimension 10 x 10 x 40 cm (width x depth x height) and is filled with water. One of the side walls is being heated, whilst the opposite wall is being cooled. Near the hot wall the water will increase in temperature, expand and move upwards. Near the cold wall the opposite happens resulting in a circulating natural convection flow inside the cavity. A two-dimensional schematic overview of the cavity and the circulating flow is shown in Figure 1.1 which is adopted from Incropera's Fundamentals of Heat and Mass Transfer [7]. The flow inside a rectangular cavity models many

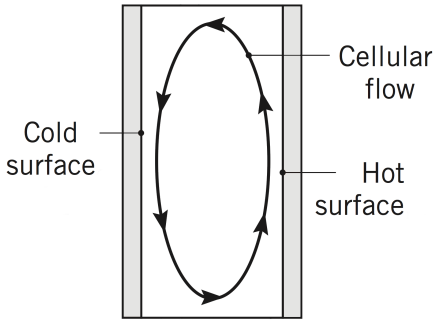

Figure 1.1: Two-dimensional schematic overview of the cavity, shown from the front side. Denoted are the hot and cold wall and circulating (cellular) flow inside the cavity.

engineering applications such as the ventilation of rooms and buildings and the cooling of electronic devices [1]. Thereby it is an important test case for numerical models and computer simulations which are used to predict heat and fluid flows [8]. When the temperature difference between the two side walls increases, so will the differences in density, resulting in larger buoyancy forces. Ultimately this leads to larger flow velocities inside the cavity. With increasing flow velocities, the characteristics of the flow will change from laminar, to transitional and fully turbulent flow phenomena. The flow inside the cavity is very sensitive to external influences and experimental conditions. All together this makes it very difficult to correctly predict the flow inside the cavity [8].

Since the natural convection flow inside a rectangular cavity is such an important benchmark, it is also a popular topic of research. The setup used in this research has been used by other researchers as well. It was build and utilized between 2010 and 2013 by André Popinhak as part of his master's thesis [3]. The flow velocity profiles he found were somewhat different from what can be expected based on the experimental and computational work from other researchers. Therefore extra measurements where required to give a clear statement regarding the results by Popinhak. The results by Popinhak and other researchers will be reviewed and compared in the literature review in Section 2.3.

The goals for this internship were to perform maintenance to get the setup back in oper-

ational condition, to redo the measurements performed by Popinhak and try to find an explanation for his somewhat anomalous results.

1.4 Dimensionless numbers

Dimensionless numbers are very useful to undo certain phenomena or problems from unnecessary context. For most applications, the quantity of a certain measure is not of importance, rather the ratio with respect to another measure is what matters. This can for instance be seen in scale models of aircraft wings in wind tunnels. By defining the position on the wing relative to the total width (chord length) of the wing, the experimental results for a small wing can be translated to a larger wing of the same shape.
In this research dimensionless numbers are used to compare results from different researchers who use different test setups in terms of dimensions, temperatures and types of fluid.

Rayleigh number Buoyancy driven flows were first studied by Bénard in 1900 [9]. He worked with very thin layers of fluid (a millimetre or less) that where heated from below and in contact with open air from above. In the fluid he discovered convection cells that where created when natural convection occurred. Each cell occupied a small volume inside the fluid where locally the fluid rises on one side of the cell and descends on the other side of the cell. Together this forms the so called cellular flow. Inspired by Bénard, Rayleigh started working on the theoretical background of this phenomena and came in 1916 with a ratio between the buoyancy on the one hand, and the viscosity and thermal conduction of the fluid on the other hand. He showed that when the ratio exceeds a certain threshold, a convective flow starts to develop. For values well below this value, heat transfer is mainly in the form of conduction [10]. This ratio found by Rayleigh is nowadays known as the Rayleigh number. It is defined in Equation 1.6 by making use of Equation 11.21 from Kundu's Fluid Mechanics as cited in [10].

$$\mathrm{Ra}_L = \frac{g\beta\Delta T L^3}{\nu\alpha} \tag{1.6}$$

In this research, the temperature difference ΔT is defined as the difference between the two heated walls $\Delta T = T_h - T_c$. The temperatures T_h and T_c are chosen 28 and 18 degree Celsius with a working (environmental) temperature T_w of 23 degree Celsius. The typical length scale L of the setup is chosen to be the height of the cavity H, which is equal to 0.4 metre. The kinematic viscosity ν of the water inside the cavity at the specified working temperature is found using extrapolation and has a value of 9.4030×10^{-7} [m^2/s] [11]. The thermal diffusivity α of the water is given by $\alpha = k/\rho C_p$ [m^2/s]. The value for the thermal conductivity k of the water was taken to be equal to 0.58 [W/(m K)] at a temperature of 25 deg Celsius [11]. The extrapolated values for the density ρ and the specific heat capacity C_p of the water inside the cavity at the specified working temperature were found to be equal to 997.44 [$\mathrm{kg/m}^3$] and 4.1803 [kJ/(kg K)] respectively [11]. Filling in these numbers results in a Rayleigh number of 1.14×10^{10}.

Prandtl number The German physicist Ludwin Prandtl (1875 - 1953) is know to be one of the founders of modern fluid mechanics. Among other things he is acknowledged for first conceiving the idea of a boundary layer; a very thin layer in which the fluid accelerates from zero velocity near the contacting surface, to the free stream velocity further away from the contacting surface. On a typical aeroplane wing with a chord of multiple metres, the maximum thickness of the boundary layer is of the order of one centimetre [10]. Similar to this velocity boundary layer, the thermal boundary layer forms the layer in which the temperature changes from the value at the contacting surface to the value further away from the contacting surface. The ratio in thickness between these two different layers is given by the Prandtl number, named after the original identifier of the boundary layers. For Prandtl numbers greater than one, the velocity boundary layer is thicker than its thermal equivalent. For Prandtl numbers smaller than one, the thermal boundary layer will be thickest. The Prandtl number is defined in Equation 1.7 by making use of Equation 4.116 from Kundu's Fluid Mechanics as cited in [10].

$$\mathrm{Pr} = \frac{\nu}{\alpha} = \frac{\mu/\rho}{k/\rho C_p} \tag{1.7}$$

From Equation 1.7, where μ denotes the dynamic viscosity [kg/(m s)] of the water, it can be seen how the thickness of the boundary layers is related to the properties of the fluid. For fluids with a high viscosity, the acceleration to the free stream velocity will require more effort, resulting in a thicker velocity boundary layer. Likewise, for fluids with a high thermal diffusivity, the heat will more rapidly move through it resulting in a more thick thermal boundary layer. For air at room temperature and standard atmospheric pressure, $\mathrm{Pr} = 0.72$, so in air the thermal boundary layer will be thicker.
Outside of the thermal boundary layer, where no heat flow is present, the temperature will be uniform. The consequence of this for the natural convection flows studied in this report, is that the variations in density, responsible for the buoyancy forces, are only present inside the thermal boundary layer. Plugging in the same values used for determining the Rayleigh number, the Prandtl number of the water used for this experiment is determined to be 6.75.

Nusselt number Another important contributor to the field of fluid mechanics is Wilhelm Nusselt (1882 - 1957). He first proposed the principal parameters in the similarity theory of heat transfer [12]. After him the Nusselt number was named. It represents the ratio between convective heat transfer and heat transfer due to conduction. For large Nusselt numbers convection is more effective. For a Nusselt number of one, heat transfer is purely in the form of conduction. The Nusselt number is defined in Equation 1.8 using Equation 5-46a from Holman's Heat Transfer as cited in [13].

$$\mathrm{Nu}_H = \frac{hH}{k} \tag{1.8}$$

The convective heat transfer coefficient h can only be determined experimentally, or by using correlations derived from experiments. Therefore it is difficult to give an exact value

for the Nusselt number. As is pointed out by Trias et al., the classical theory assumes that the Nusselt number scales with approximately $Ra^{1/4}$ for laminar flow and with $Ra^{1/3}$ for turbulent flow [14]. For different flow geometries and regimes formulations for the Nusselt number are found using experimental studies. Çengel gives, in his section on vertical rectangular enclosures, some of these formulas that can be used to determine the Nusselt number [6]. Most suitable for our setup is Equation 9-53 (as cited in [6]), which gives the Nusselt number as

$$\mathrm{Nu} = 0.22 \left(\frac{Pr}{0.2 + Pr} Ra_H \right)^{0.28} \left(\frac{H}{W} \right)^{-1/4} \tag{1.9}$$

which is valid for aspect ratios (height versus width of the cavity) of $2 < H/W < 10$, any Prandtl number and $Ra_H < 10^{10}$. Filling in results in a Nusselt number of 101 for the experiment discussed in this report.

Grashof number As was mentioned before, viscous forces counteract the movement of the flow. A relation between the buoyancy force and viscous forces acting on the fluid is given by the Grashof number, named after the German engineer Franz Grashof (1826-1893) [12]. The Grashof number is defined in Equation 1.10 using Equation 9-15 from Çengels's Heat Transfer [6].

$$\mathrm{Gr}_H = \frac{g\beta\Delta T H^3}{\nu^2} \tag{1.10}$$

Note that the product of the Grashof and the Nusselt number equals the Rayeigh number. Filling in the values for our setup as given above results in a Grashof number of 1.68×10^9. According to Çengel, for values of the Grashof number above 10^9 the flow over a vertical plate becomes turbulent [6]. Therefore it is suspected that the flow observed in this research is in the transitional regime between laminar and fully turbulent flow.

Chapter 2

Theoretical background

2.1 Governing equations

The equations governing the motion of a fluid are derived from the three fundamental conservation laws of physics; the conservation of mass, the conservation of momentum and the conservation of energy. Thereby the assumptions are made that the fluid is a continuum, so it is not considered as an assembly of individual particles or molecules. The fluid is also assumed to be uniform and homogeneous, so it has the same composition everywhere.

Continuity The continuity equation is based on the conservation of mass. It is valid at all times for all volumes and infinitesimal points in the fluid. In PDE-conservation form the continuity equation is given by

$$\frac{\partial}{\partial t}\rho + \nabla \cdot \rho\vec{u} = 0 \tag{2.1}$$

where $\vec{u}$ is the fluid velocity vector [m/s]. The $\frac{\partial}{\partial t}\rho$-term on the left represents the increase of mass per unit time. The $\nabla \cdot \rho\vec{u}$-term stands for the mass flux due to the velocity of the flow. Together they equal zero, thus stating that mass can neither be created nor destroyed. Consider for instance a fixed volume in a flow; the difference between the mass flowing in at one side of the volume and the amount of mass flowing out at the other side of the volume should be equal to the change of mass inside the volume.

Momentum The momentum equation (or Navier-Stokes equation) is based on Newton's second law; $\vec{F} = m\vec{a}$. It sums al the forces working on the fluid and is given in PDE-conservation form by

$$\frac{\partial}{\partial t}\rho\vec{u} + \nabla \cdot \rho\vec{u}\vec{u} = \rho\vec{f} - \nabla p + \nabla \cdot \bar{\bar{\tau}} \tag{2.2}$$

With the momentum defined as $\rho\vec{u}$, the left hand side of Eq. 2.2 looks similar to the LHS (left hand side) of Eq. 2.1. It thus represents the increase of momentum per unit time and the momentum flux due to the velocity of the flow. The first term on the RHS represents

the external (or body) forces working on the fluid. Examples are the gravity force and the Coriolis force which is present in a rotating frame of reference. The two terms on the RHS represent the surface forces. These forces are imposed by the surroundings of the fluid. The first term $-\nabla p$ represents the static pressure [N/m^2]. The second term features the viscous stress tensor $\bar{\bar{\tau}}$ [kg/ms^2] which holds the terms of the normal and shear stresses acting on the fluid.

Energy The energy equation is based on the first law of thermodynamics which states that energy is conserved. In PDE-conservation form it is given by

$$\frac{\partial}{\partial t}\rho E + \nabla \cdot \rho \vec{u} E = \rho \vec{u} \cdot \vec{f} - \nabla \cdot p\vec{u} + \nabla \cdot \bar{\bar{\tau}}\vec{u} + \dot{Q} - \nabla \cdot \vec{q} \tag{2.3}$$

The two terms on the LHS represent the increase of energy per unit time and the energy flux due to the velocity of the flow. The first three terms on the RHS represent the work carried out by the body and surface forces. The last two terms on the RHS represent heating by external sources. such as the absorption or emission of heat due to radiation. The term $\dot{Q}$ represents the heat sources [J/m^3] and $\vec{q}$ is the heat flux vector [J/m^2].

2.2 Exact solution

By imposing simplifications and assumptions on the flow inside the cavity, it is possible to derive an exact solution to the problem. To do so, the cavity is considered to be of infinite height and depth, with the hot and cold wall a distance $2B$ apart on the x-axis. This makes the problem two-dimensional. The temperature of the hot wall is T_h and for the cold wall this is T_c. Both are independent of the height (y-axis) of the cavity. Other assumptions include steady state and incompressible flow.
Since the flow velocity in the x-direction will be much smaller than the velocity in y-direction, the x-component of the flow velocity is neglected. The result of this, is that the transport of energy in the x-direction will therefore be only due to conduction. Due to the steady state assumption, the amount of conductive heat transfer per area in the x-direction is constant and is given in Equation 2.4, which is adapted from Equation 1.2.

$$\frac{dQ_{cond}}{dx} = 0 \rightarrow -k\frac{d^2T}{dx^2} = 0 \tag{2.4}$$

Solving this and applying the temperature boundary conditions for the hot and cold wall results in the expression for the temperature distribution.

$$T(x) = T_\infty - \frac{\Delta T}{2B}x \tag{2.5}$$

To find the velocity distribution the momentum equation is used. Because of the assumptions of steady state and incompressible flow, the momentum equation in Equation 2.2 can be reduced to Equation 2.6. This equation is valid for an incompressible flow on which the steady state assumption is applied.

$$\rho \vec{u} \cdot \nabla \vec{u} = \rho \vec{g} - \nabla p + \mu \nabla^2 \vec{u} \tag{2.6}$$

Or, written in tensor notation in Equation 2.7.

$$\rho u_j \frac{\partial u_i}{\partial x_j} = \rho g_i - \frac{\partial p}{\partial x_i} + \mu \frac{\partial^2 u_i}{\partial x_j^2} \tag{2.7}$$

Here the body forces are taken to be consisting of the gravitational force only. Since the velocities in x- and z-direction are considered to be negligible, only the PDE describing the velocity in y-direction is of interest. Simplifying and expanding Equation 2.7 results in Equation 2.8 for the vertical fluid velocity.

$$\rho \left(u_x \frac{\partial u_y}{\partial x} + u_y \frac{\partial u_y}{\partial y} + u_z \frac{\partial u_y}{\partial z} \right) = -\rho g - \frac{\partial p}{\partial y} + \mu \left(\frac{\partial^2 u_y}{\partial x^2} + \frac{\partial^2 u_y}{\partial y^2} + \frac{\partial^2 u_y}{\partial z^2} \right) \tag{2.8}$$

Since the velocities u_x and u_z can be considered zero and u_y only varies with x, this equation is simplified to Equation 2.9.

$$\mu \frac{\partial^2 u_y}{\partial x^2} = \frac{\partial p}{\partial y} + \rho g \tag{2.9}$$

The density term ρ in Equation 2.9 is varying dependent of the temperature. After all, the variation in density is the driving force in natural convection flows. Here the Boussinesq approximation is used which states that (for certain cases) the density changes in a fluid can be neglected except where the density ρ is multiplied with the gravity g [10]. Since the temperature distribution is known, the volume expansion coefficient β can be used to determine the variations in density. The volume expansion coefficient is a fluid property which relates the change in temperature to the change in density. It is defined in Equation 2.10, using Equation 9-3 of Çengel's Heat Transfer as cited in [6].

$$\beta = \frac{1}{v} \left(\frac{\partial v}{\partial T} \right)_P = -\frac{1}{\rho} \left(\frac{\partial \rho}{\partial T} \right)_P \tag{2.10}$$

Here the underscore P denotes constant pressure. A Taylor expansion of ρ with respect to the temperature around $T_\infty = \frac{1}{2}(T_h + T_c)$ using Equation 2.10 gives

$$\rho = \rho_\infty + \frac{\partial \rho}{\partial T}(T - T_\infty) + ... \tag{2.11}$$

$$= \rho_\infty - \rho_\infty \beta (T - T_\infty) \tag{2.12}$$

Plugging in Equation 2.9 results in

$$\mu \frac{\partial^2 u_y}{\partial x^2} = \frac{\partial p}{\partial y} + \rho_\infty g - \rho_\infty g \beta (T - T_\infty) \tag{2.13}$$

Note that now in Equation 2.13 the density is constant and the variation in density is replaced by the temperature difference. Plugging in the expression for the temperature distribution in the cavity equation found above (Equation 2.5), the ODE that describes the vertical fluid velocity in the cavity becomes as given in Equation 2.14.

$$\mu \frac{\partial^2 u_y}{\partial x^2} = \frac{\partial p}{\partial y} + \rho g + \frac{1}{2} \rho g \beta \Delta T \frac{x}{B} \tag{2.14}$$

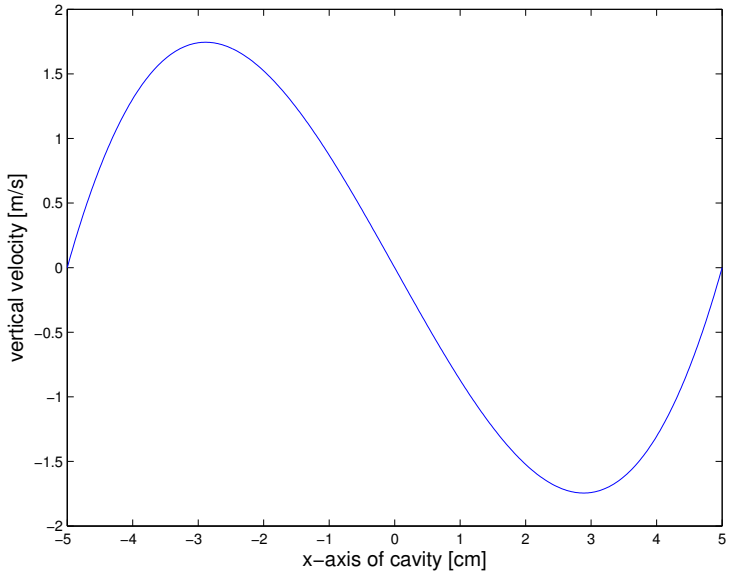

Figure 2.1: Distribution of the vertical velocity inside the cavity, solved exactly using an extremely simplified model assuming a cavity of infinite aspect ratio.

This equation shows the balance between the frictional forces on the LHS and the pressure and both the gravitational and buoyancy forces on the RHS. The no-slip conditions provides the two boundary conditions required for solving the ODE stating that the vertical velocity at the walls is zero.
The solution to Equation 2.14 is given in Equation 2.15, stating the vertical flow velocity dependent of the x-position in the cavity. It is adopted from Equation 10.9-15 of Bird's Transport Phenomena as cited in [15].

$$u_y = \frac{\rho g \beta \Delta T B^2}{12\mu} \left[\left(\frac{x}{B}\right)^3 - \left(\frac{x}{B}\right) \right] \tag{2.15}$$

Equation 2.15 is plotted using MATLAB resulting in the graph shown in Figure 2.1. The average velocity of the upward direction is found to be equal to 1.13 m/s, whilst the maximum velocity lies about 1.7 m/s. When this is compared with for instance the experimental work by Popinhak as shown in Figure A.1, it can be concluded that the assumptions made in determining an exact solution are of great influence. Popinhak finds for a cavity of AR (aspect ratio) 4 a maximum velocity of about 8.5 mm/s, depending of the height at which is measured in the cavity. The maximum of 8.5 mm/s is reached at half cavity height. For the exact solution infinite walls are assumed, so the AR becomes infinite and the influence of the height of measurement is lost. Also, the turbulent flow phenomena that are observed by Popinhak are not taken into account due to the steady state assumption.
Although the results from the exact solution are not very useful, its derivation provides a good insight in the important mechanisms involved in the cavity flow. The balance

between the driving buoyancy force and the counteracting frictional, gravitational and pressure is shown clearly in Equation 2.14.

2.3 Literature review

Natural convection flows in a differentially heated cavity has been the subject of research for the past decades. It models the flow of many engineering applications such as airflow inside a room, the cooling of electronic devices and even nuclear reactors [1]. Thereby it can also function as a benchmark problem to validate numerical models. Research has presented itself in many forms, including experiments with different types of cavities in terms of aspect ratios and fluids (Prandtl numbers) being measured under different inclinations [16–21]. In the past decade, the increase in computational power made it more interesting to perform three-dimensional CFD simulations and work with higher Rayleigh numbers entering the turbulent regime.

Experimental work The first publication on the subject of fluids inside cavities with differentially heated side walls is considered to be from Wilhelm Nusselt in 1909 [22]. In the first half on the 20th century experimental work was performed by different authors, mainly aimed at measuring the amount of heat transported from the hot to the cold wall. It was found that for higher Grashof numbers the expression of the Nusselt number changed, which was interpreted as an indication of a transition from laminar to turbulent flow [23]. In 1954 G.K. Batchelor stated in an analytical study that various flow regimes exist depending on Rayleigh number and geometry [24]. Batchelor concluded that for low Rayleigh numbers boundary layers are thin and heat is mainly transported via conduction. For larger Rayleigh numbers, the boundary layers are to build up in thickness. Batchelor also believed that inside the cavity a core of uniform temperature and vorticity would be created when the Rayleigh number approaches infinity [23].
The different types of flow depending on Rayleigh number as suggested by Batchelor are pictured in Figure. 2.2, which is adopted from Figure 7.9 from Holman's Heat Transfer as cited in [13].

In 1990, Penot et al. showed that for a cavity with AR 4, the critical Rayleigh number, denoting the transition from laminar to turbulent cavity flow, is $1.57\times10^6 \pm 5\%$ [25]. This is well in accordance with Figure 2.2 where the critical regime is between Rayleigh number values of 10^6 and 10^7. Later in 2010, Penot et al. describe secondary flows at the top and bottom walls of the cavity for Rayleigh numbers of 9.2×10^7 [26]. The secondary flows appear in the form of recirculating flows (vortices) in the top and bottom regions of the cavity. In 2013, Popinhak found secondary flows occurring at a Rayleigh number of 1.14×10^{10} in the formation of vortices at the top and bottom corners near the hot, respectively cold wall [3]. This was explained by Popinhak to be caused by the fluid changing direction after encounter with the top and bottom walls, resulting in the formation of a vortex. Since these vortices are not present in time averaged flows, he concluded this to be an issue of permanent flow unsteadiness [3]. The vortices travel with the direction of

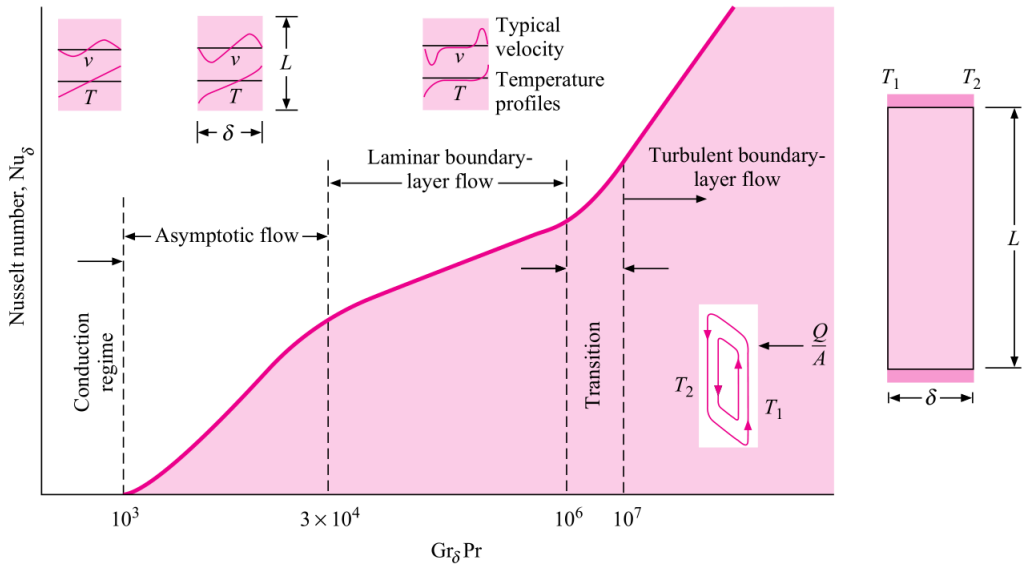

Figure 2.2: Overview of different flow regimes, shown with dependency on Rayleigh number with accompanying Nusselt number [13].

the flow related to the nearest wall; so upwards near the hot wall and downwards near the cold wall. These vortices were particularly visible near the cold wall. The flow velocity near the cold wall changed with increasing distance to the cold wall from negative, to positive again to negative before converging to zero. This is most clear in Figure A.1e in Section A, which holds the results from Popinhak [3]. Here at half-cavity height the velocity profile near the cold wall closely resembles a symmetrical sinus wave.

In 2011, Saury et al. performed measurements at high Rayleigh numbers ranging between 4.0×10^{10} and 1.2×10^{11}, finding phenomena similar to Popinhak and Penot et al. [4]. Near the top and the bottom of the cavity, a recirculating flow was seen between the hot and the cold walls, resembling the secondary flows described by Penot et al. [26]. At distances above 0.8 cavity height (height expressed as a fraction of the total height of the cavity, measured from the bottom) the rising flow near the hot wall was reported to take a 'short-cut'. At this point the flow was seen to cross to the cold side of the cavity before reaching the top of the hot side [4]. The strong vortices in the top and bottom corners as found by Popinhak are not reported by Saury et al. [3]. The weak back flow at the hot wall side where the velocity changes sign whilst converging to zero, present in the results from Popinhak, are also reported by Saury et al. [3]. In the results from Popinhak this backflow appears strongest in Figures A.1e - A.1h in Section A. The almost sinusoidal flow near the cold wall reported by Popinhak is not presented by Saury et al. [3]. Also, in Popinhak's work, the absolute velocities at the cold wall side are very small compared to the absolute velocities at the hot wall side [3]. The results by Saury et al. show a more symmetric flow profile, not only in terms of shape, but also in terms of maximum absolute velocity

between the hot and the cold wall side [4].

Numerical research In Section 2.2 it is concluded that no simple exact solution can be found for the cavity problem. This is the case for the majority of the more complicated flows and geometries. Numerical (computer) simulations are used to makes predictions regarding the flow of these more complicated cases. Advantages of numerical simulations include that it is usually faster and cheaper to run simulations than to do (scaled) experiments. Thereby certain conditions that are rather to be avoided in real live experiments can be simulated using computational fluid dynamics (CFD). Examples are explosions and the spread of pollutant in the atmosphere.
Where an exact solution solves the problem on a continuous domain, CFD only solves the problem at certain points chosen in the domain. The number and distribution of points chosen is of influence of the accuracy of the solution. It is important to always keep in mind that a CFD simulation gives just a prediction of the flow and that accuracy is always questionable. This can be due to human error, involving to much guessing or errors by choosing input data, as well as because of limitations of computational power requiring simplified models.

An overview of numerical research on differentially heated cavities is given by Trias et al. [2]. They credit Vahl Davis and Jones for the formulation of the original benchmark problem for two-dimensional (2D) square cavities in 1983. Their research focussed on the laminar regime with Rayleigh numbers between 10^3 and 10^6. After their pioneering work the research can be organized in multiple groups, corresponding to flow regime, cavity aspect ratio, type of boundary condition used and 2D or 3D simulations. Only results relevant to the cavity problem for this report are discussed, for a more complete overview the reader is referred to [2].

Increased computational power makes it possible to simulate higher Rayleigh numbers and 3D flow effects in cavities. A distinction is made between cavities with solid vertical front and back walls and cavities with periodic vertical boundary conditions, thus resulting in a cavity of infinite depth. Although more closely related to real life experiments, the cavity with solid vertical walls is a less popular topic in numerical research [2]. The cavity with periodic boundary conditions is of more interest due to its higher computational efficiency. This is due to the near wall effects of the vertical, non-heated front and back wall that are not taken into account in the simulation. At distances further away from these walls, beyond the thermal and velocity boundary layers, the solution will however be able to give correct predictions regarding the flow behaviour. In this configuration the flow is not forced to be 3D. Dependent of Rayleigh number three different types of flow are possible; 2D laminar, 2D turbulent and 3D turbulent [2]. Depending on AR, the transition from 2D laminar to 3D turbulent flow occurs directly or via the 2D turbulent regime, which only exists for a small range of Rayleigh numbers. For all AR the transition to unsteady (turbulent) flow behaviour occurs for Rayleigh numbers of the order 10^8 [2]. The Rayleigh

number for transition to turbulence found in experimental work is much lower than this value. For this transition Penot et al. found a Rayleigh number of the order 10^6, a factor 100 lower. This difference might be caused by the periodic vertical boundary conditions imposed on the front and back wall of the cavity. For the cavity with solid vertical walls, the transition to turbulence was studied by Janssen et al. who found a critical Rayleigh number between 2.25×10^6 and 2.35×10^6, using perfectly conducting horizontal walls and imposing flow symmetry [27]. However, for adiabatic horizontal walls Janssen and Henkes found a critical Rayleigh number between 2.5×10^8 and 3×10^8 [28]. For a similar case without assuming symmetry, Labrosse et al. found a critical Rayleigh number of 3.19×10^7 [29]. This illustrates the influence of input data on the outcome of CFD simulations and emphasizes the need to be alert when analysing CFD results.

In the laminar and transitional flow regime, a 2D simulation is sometimes sufficient to predict the flow inside the cavity. For the turbulent regime however, this is not the case. In 2007 Trias et al. performed DNS (direct numerical simulation) simulations with Rayleigh numbers up to 10^{10}, finding significant differences between 2D and 3D results. The large unsteady eddies (vortices) found in the 2D simulations exist only for short periods of time in the 3D simulations. In 3D their energy is quickly dissipated to smaller scales of turbulent motion, reducing the effect of mixing at the top and bottom of the cavity. The result of this is that the core (center) of the cavity remains motionless, consisting out of multiple layers of temperature [30]. So the predictions made by G.K. Batchelor in 1954 were very accurate, although he belied a core of uniform temperature would be formed for Rayleigh numbers reaching infinity [23]. Concluded by Trias et al. was that 3D simulations are necessary when working in the turbulent regime [2].

For all of the cavity setups reviewed here, air was used as a working fluid to fill the cavity. Our setup however features a water filled cavity. Air holds a Prandtl number of 0.71, whereas the Prandtl number for our setup was determined to be 6.75 in Section 1.4. In 1995, the influence of the Prandtl on instability mechanisms and transition to turbulence was researched by Janssen and Henkes [31]. Their main conclusion was that for Prandtl numbers between 0.25 and 2.0 (which includes air), the transition from laminar to turbulent flow consists out of several stages. For Prandtl numbers between 2.5 and 7.0 (including water) however, this transition is instantaneous. They attribute this difference in transitional behaviour to a difference in the instability in the vertical boundary layers which causes the turbulent behaviour. For the lower Prandtl number range ($\mathrm{Pr} \leq 2$) this instability is periodic in time, whilst in the higher Prandtl number region it is chaotic [31]. Since the flows studied in this report are well in the turbulent regime, the difference in Prandtl number is not considered to be of great influence.

Direct numerical simulations in a 3D cavity of aspect ratio 4 with Rayleigh numbers up to 10^{11} in the turbulent regime were performed by Trias et al. [2, 14]. The AR and Rayleigh number studied by Trias et al. match very closely with the experimental setup studied in this report ($\mathrm{AR} = 4$, $\mathrm{Ra} = 1.14\times10^{10}$). What is shown very clearly by Trias et al. is

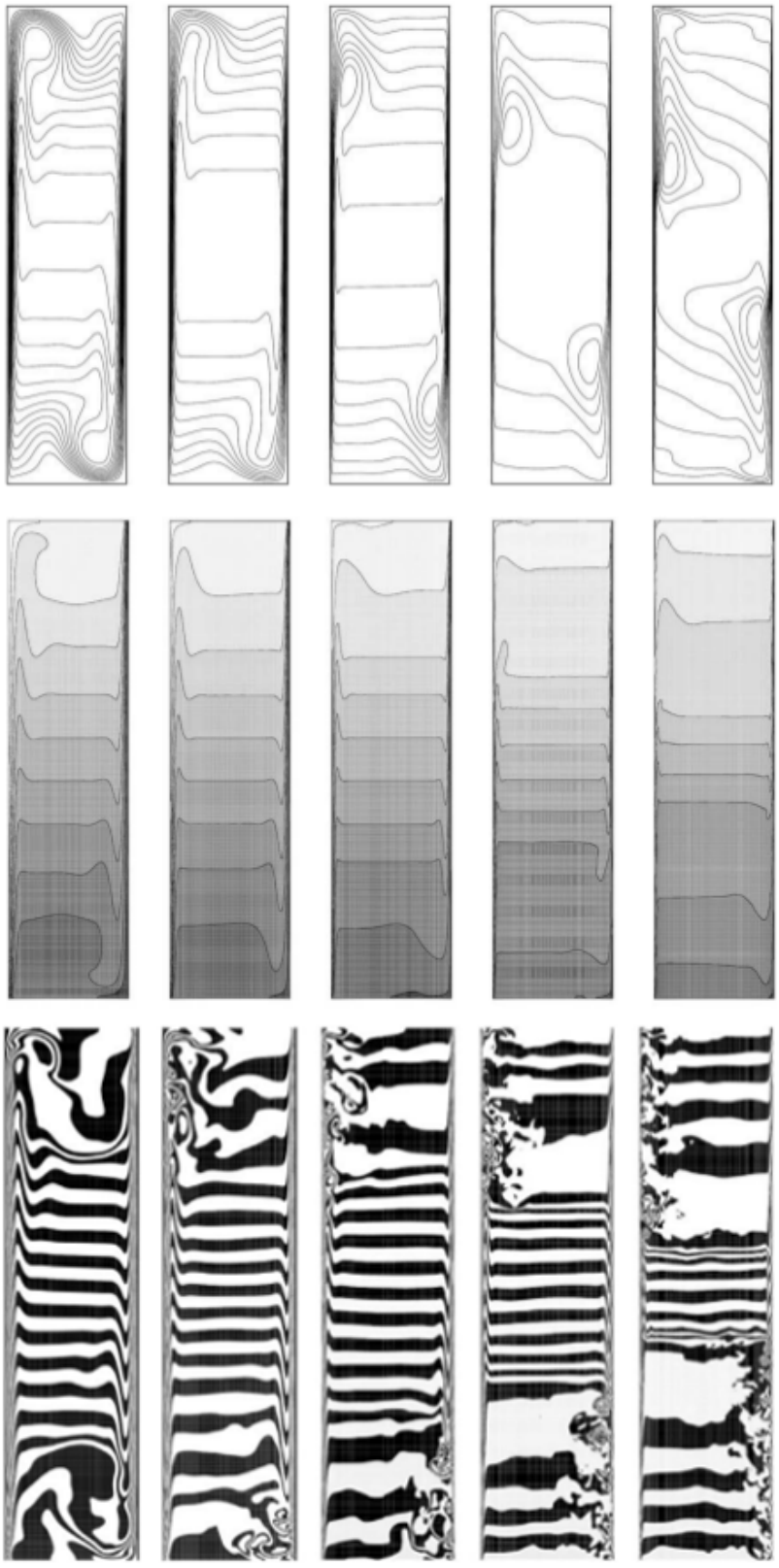

Figure 2.3: DNS results by Trias et al. for a differentially heated cavity with AR 4. From left to right: Ra = 6.4×10^8, 2×10^9, 1×10^{10}, 3×10^{10} and 1×10^{11}. Shown are the streamlines of the averaged flow (top), the average temperature field with uniform distributed isotherms (middle) and the instanteneous (non averaged) temperature field with uniform distributed isotherms (bottom) [2, 14].

that with increasing Rayleigh number, the position where the boundary layer separates from the wall and the flow becomes turbulent moves further upstream. This is shown in Figure 2.3, which is adopted from Trias et al. as cited in [2]. This is in accordance with the experimental results by Saury et al. as discussed in the first part of Section 2.3. They state that for higher Rayleigh numbers the flow is turbulent at a certain position in the cavity, whilst it is laminar at the same position for lower Rayleigh numbers [4]. Although Saury et al. draw no clear conclusions from this, it could indicate that with increasing Rayleigh number, the point where the boundary layers separates from the wall moves further upstream.
Notice that the flows with different Rayleigh numbers display similar characters; thin vertical boundary layers, a core with a very low time averaged velocity and a stratified (stacked) temperature distribution. It can also be seen that with increasing Rayleigh number, the temperature distribution becomes less uniform. This results in a core with a relatively large vertical temperature gradient, whilst at the top and bottom of the cavity the thermal layers grow larger.

The simulation that shows the most resemblance with the cavity studied in this research ($Ra = 1.14\times10^{10}$) is the one with Rayleigh number 1×10^{10}. A Rayleigh number of 1×10^{10} corresponds in our setup to a temperature difference between the hot and the cold wall of 8.8 degree Celsius, whilst 1.14×10^{10} corresponds to to a temperature difference of 10 degree Celsius. Thereby, since both Rayleigh numbers are well above the previously discussed 10^6 and 10^8, it can be safely assumed that both are well in the turbulent regime. The similarity between the simulation and the experiment is confirmed by comparing the Nusselt number found by Trias et al. to the one obtained using Eq. 1.9; 101.94 versus 101 [14]. The difference between the simulation and our setup is in the Prandtl number associated to the fluid inside the cavity. Trias et al. use air as a working fluid with a Prandtl number of 0.71. The cavity used in this research, the same as was used by Popinhak, features water with a Prandtl number of 6.75. Based on the research by Janssen and Henkes this is not assumed to be of major influence. Their findings suggest that the size of the Prandtl number is mainly of influence on the transition from the laminar to the turbulent flow regime [31]. Therefore it is assumed that once the turbulent regime is entered the influence of the Prandtl number is negligible.
The setup used for the experiments described in this report is the same as used by Popinhak [3]. Therefore his results can also be compared with the numerical results by Trias et al. [2, 14]. Popinhak found a strong backflow and relatively small absolute velocities near the cold wall side as is shown in Figure A.1 in Section A [3]. This could correspond to the turbulent regions visualized by Trias et al. in the top plot of Figure 2.3 [2]. This effect is however missing from the results of Popinhak near the hot wall, which show more resemblance to the near hot wall results from Saury et al. as cited in [4].

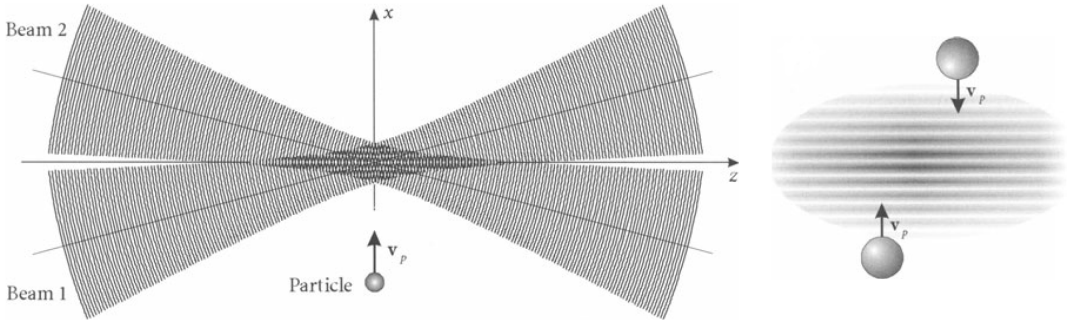

Figure 2.4: Interference pattern of two crossing laser beams. The left image shows the crossing of the two beams, the right image is a close up of the refraction area [32].

2.4 Laser Doppler velocimetry

A TSI Laser Doppler velocimetry (LDV) system is used to measure the flow inside the cavity. LDV is a relatively young technique first introduced in the 1970's. LDV is widely used in the field of fluid mechanics due to its attractive characteristics including non-intrusiveness, directional sensitivity, high accuracy and high spatial and temporal resolution [32]. To be able to set up and operate a LDV system correctly it is important to have some basic knowledge on the theory behind its operation.

When light is thought of as a traveling wave, it is not difficult to imagine that where two beams of light meet, an interference pattern is created. Depending on the phase differences between the two waves there is constructive interference (when two crests meet each other) resulting in a bright spot, or destructive interference (when a crest and a trough meet) resulting in a dark spot. This results in a pattern as shown in Figure 2.4. When a particles crosses this interference pattern it will scatter the light of the two interfering laser beams. When this scattered light falls upon a detector, the difference in intensity of the scattered light can be used to determine the velocity of the particle [32]. The time difference between two intensity peaks Δt in the signal scattered by the particle corresponds to the distance the particle has to travel between two bright spots of the interference pattern. This distance Δs is related to the known wavelength of the laser beams. So the velocity normal to the lines of the interference pattern is determined by

$$v_n = \frac{\Delta s}{\Delta t} \tag{2.16}$$

When all the lines of the interference pattern are used to increase the accuracy, Equation 2.16 changes into

$$v_n = \frac{\Delta s}{T} = f_{doppler} \Delta s \tag{2.17}$$

Where T is the period between intensity peaks and $f_{doppler}$ is the frequency of the signal scattered by the particle.

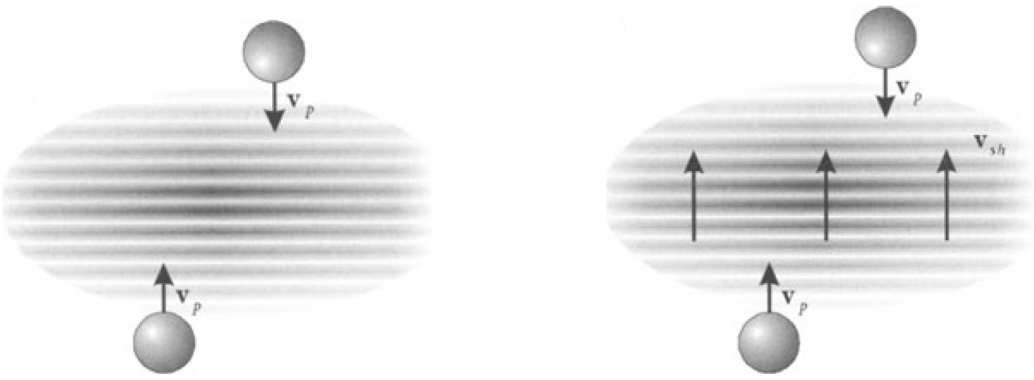

Figure 2.5: Refraction area of two laserbundels with the same wavelength (left) and for two laserbundles with different wavelengts (right) which results in the movement of the bright and dark spots over the refraction area [32].

Using this technique the magnitude of the velocity can be determined, but it is still not know if the particle in Figure 2.4 is moving either up or downwards. To be able to make this distinction, two incident laser beams with different wavelengths are used. This will result in a constantly changing interference pattern, since the crests of the two waves continuously encounter each other at different positions. The bright spots of the interference pattern are therefore moving with a constant velocity, which is graphically represented in Figure 2.5. Due to the Doppler effect, a particle moving in the same direction as the bright areas of the interference pattern will scatter light at a lower frequency. A particle moving in the opposite direction will scatter light at a higher frequency.

The scattered light has to be filtered from any noise that has been picked up along the way to the receiver. To be able to do this correctly, it is important to be aware of the frequency difference between the two bundles creating the measurement area. The frequency captured by the receiver is given by Equation 2.18 which is adapted from Equation 2.33 from Albrecht's Laser Doppler and Phase Doppler Measurement Techniques [32].

$$f_{signal} = f_{shift} + (\text{sign}(v) \cdot f_{doppler}) \tag{2.18}$$

From Equation 2.18 it can be seen that the negative velocities will feature a frequency lower than f_{shift}, while the positive velocities will display a frequency higher than f_{shift}.

To clarify this formula, an example is given which is applicable to the cavity problem studied in this report. In this setup the frequency shift is known to be 40 MHz. From earlier work and literature research, the flow velocities inside the cavity are estimated between -10 and 10 [mm/s]. The frequency of the captured signal can be determined using Equation 2.17. Using a value of 3.73 μm for Δs, a frequency range between -2.7 and 2.7 kHz is found. Filling in for Equation 2.18 gives

$$f_{signal} = 40 \text{ MHz} \pm 2.7 \text{ kHz} \tag{2.19}$$

The frequency of f_{signal} ranges between 39997.3 and 40002.7 kHz. Since only fixed filters are available in the LDV setup used in this research, the frequency of f_{signal} has to be adjusted to fit within an available filter range. This process is called downmixing. Since the frequency range of interest has a width of 5.4 kHz, the filter which permits frequencies between 1 and 10 kHz is most suitable in this example.
To be able to fit f_{signal} inside this frequency band, it has to be downmixed with a value of 39994.5 kHz. When this downmix frequency is subtracted from the original f_{signal}, the resulting range is 2.8 - 8.2 kHz, well within the specified frequency band.

Chapter 3

The experiment

The goal of this research is to study natural convection flows in a closed cavity with differentially heated side walls. Therefore a setup is used where the flow inside a water filled cavity is measured using Laser Doppler velocimetry.

3.1 Experimental setup

A schematic overview from the side of the setup is adopted from Figure 3.2-1 from the work by Popinhak (as cited in [3]) and is shown in Figure 3.1. The individual components are when necessary explained in further detail.

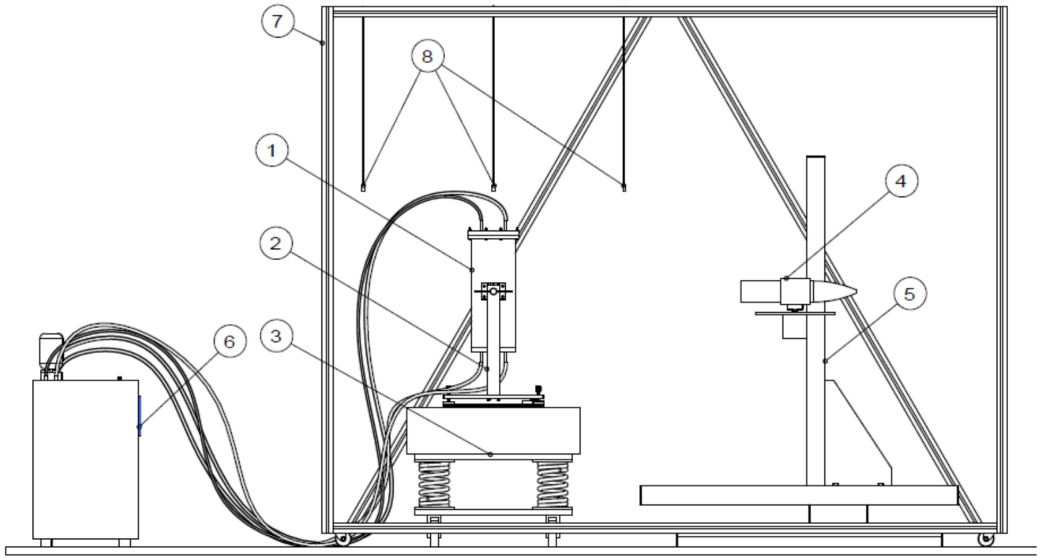

Figure 3.1: Schematic overview of the setup consisting of the following components; (1) cavity, (2) support, (3) vibriation isolator, (4) LDV scope, (5) traverse, (6) thermostatic baths, (7) tent, (8) thermocouples [3].

Cavity The cavity used in the experimental setup has dimensions of 10 x 10 x 40 mm (width x depth x height). It is made out of thick acrylic glass to ensure a minimum in heat loss (k = 0.20 W/(m K) [33]) and a low absorption of the laser light (transmittancy $\approx$ 90% [33]) used to measure the velocity of the flow. Due to the height of the cavity and the temperature difference between the side walls, using Equation 1.6, the Rayleigh number is found to be equal to 1.14 $\times 10^{10}$. The support of the cavity is designed in such a way that the inclination of the cavity can be easily altered. To reduce the influence of external vibrations the support is designed to be as stiff as possible. The support consists of two aluminium pillars attached to an aluminium plate as can be seen on the photo of the cavity and its support in Figure 3.2. The aluminium plate lies on top of another aluminium plate. The inclination between these two plates can be adjusted using two precision screws. The cavity itself can also be rotated over the x-axis with respect to the pillars. The aluminium stacked structure lies on top of a heavy ($\pm$ 20 kg) iron plate which rests on top of a 200 kg concrete block. The block is supported by four spring isolators. The cavity is supported in this way to lower the eigenfrequency of the experimental setup and to ensure its stability [3].

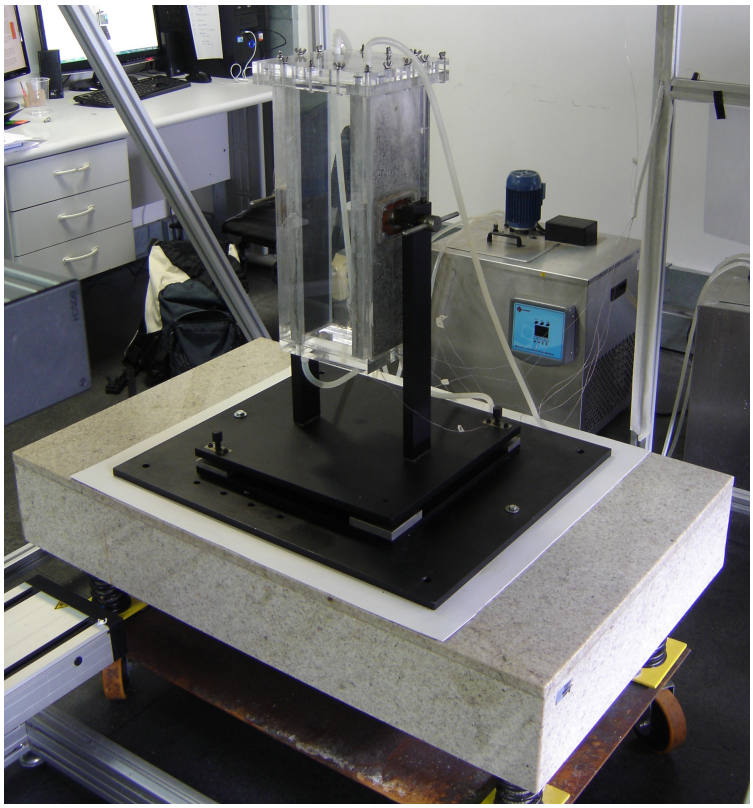

Figure 3.2: Representational overview of the setup.

Seeding particles The cavity is filled with deionized water while ensuring a minimum of air bubbles being trapped inside the cavity. Small polyamid particles are added to the water which follow the trajectory of the flow. Their movement can be observed and measured more easily than the movement of the much smaller water molecules. To give a reliable representation of the flow inside the cavity it is important that the particles have the same density as the water has. The correct amount of particles is important, as will be shown in Sections 4.1 and 5.1. The particles used are commercially available Polyamid Seeding Particles (PSP) from the Dantec Dynamics company. They have a diameter of 5 μm and hold a density of 1.03 kg/L.

Baths The temperature of the walls is controlled using thermostatic baths with an integrated pump. They are filled with about 8 litres of deionized water each. The exits of the baths are connected to the top of the heated walls. The inlets are connected to the bottom of the walls, forming a closed circuit.

Thermocouples The temperature in the walls and the surroundings are monitored using 10 thermocouples. Six of them are installed at different heights in the heated walls. The remaining four are mounted above the cavity, soldered to a small lump of metal to act as a heat buffer. They are calibrated using the thermostatic baths and a certified calibrated thermometer.

Laser Doppler velocimetry A TSI Laser Doppler velocimetry (LDV) system is used to measure the flow. The theory behind the LDV technique is explained in further detail in Section 2.4. The LDV system consists of multiple components. The laser light is generated by a Coherent Innova 70c-2 ion laser with a mixed wavelength output. It is cooled via a closed circuit using a Mecalor UMAG cooler. The wavelengths from the laser are split using a TSI FBL-3 Fiberlight multicolour Beam Separator. It uses a prism to separate the different colours of the laser beam and a Bragg cell to create the frequency shift of 40 MHz that was introduced in Section 2.4. A schematic overview of the operation of the beam separator is shown in Figure 3.3, adopted from one of the TSI online seminars as cited in [34]. In this research only the green (514.5 nm) and the blue (488 nm) light are used, since 2-dimensional measurements are performed.

After the beam separator, the light is projected on the cavity using a TSI TR60 TLN06-363 scope. In the measurement volume the shifted and unshifted beams cross each other at an angle of 7.9 degree, the lens focal distance is 349.7 mm. The interference pattern created consists out of 24 fringes per dimension. The spacing between fringes is 3.73 and 3.54 μm for the green and blue light respectively [35].

The scope also acts as the receiving optic for the light scattered by the seeding particles. Each time a particle passes through the measurement volume, it scatters light which can be detected. The number of detected passages and total passages per second is dependent of the particle density in the flow, the local flow speed, quality of the signal and external

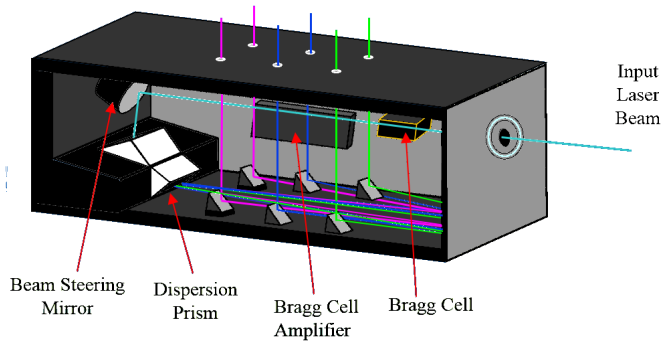

Figure 3.3: Schematic overview of the TSI beam seperator. The incoming laser beam is split into three different colors, each color consisting of a shifted and unshifted beam [34].

light sources. In the setup used in this research, an average data rate of about 5 measurements per second was achieved. The signal received by the probe is amplified and high-pass filtered by a TSI PDM 1000 photo detector module. The amplified signal passes through a TSI FSA 4000 signal processor where its frequencies are filtered and shifted depending on the settings that were passed to the TSI FlowSizer computer software.

The LDV system and the traverse are controlled using the FlowSizer software supplied with the LDV system. It can perform scheduled measurements, where a grid of certain positions is coupled to certain systems settings such as the maximum measurement time for each position and the settings regarding the filtering and shifting of the incoming signal. The grids containing the positions are created using Excel and the files containing the settings are generated by FlowSizer itself and when necessary adjusted using Notepad. The measured frequency, calculated velocity and measurement position are exported and imported in MATLAB. From this data average velocities per measurement position are calculated and a flow profile is plotted. Apart from this, the average velocity per number of measurement is calculated to gain insight in the minimum number of measurements per position required to get reliable results.

Traverse The LDV scope is mounted on a TSI 3D traverse system. It offers an accuracy of $\pm$ 300 μm and a repeatability of $\pm$ 10 μm [36].

Tent The cavity and the traverse are placed inside a aluminium framed box which can be closed using black curtains. Apart from to protect the outside from possible laser reflections, it also protects the seeding particles in the cavity from outside light that can be scattered by the seeding particles and influences the measurements.

3.2 Experimental procedure and settings

An extensive measurement manual was written to be of assistance to future students and researchers working with the cavity and LDV equipment. Therefore only a short overview of the measurement procedure will be presented in this section.

With the cavity carefully being filled with the correct amount of particles it was made sure that it was levelled using an inclinometer. The position relative to the laser was checked using a shooting target attached to the cavity and the four laser bundles from the scope; With the scope moving backwards, the four dots corresponding to the laser bundles were to move from the center of the target to the same circle around it.
The thermostatic baths operated at 18 and 28 degree Celsius in order to obtain a temperature difference of 10 degree Celsius in the cavity. An air-conditioner system was used to keep the surrounding temperature at 23 degree Celsius to ensure a minimum in heat losses from the cavity. The temperature of the walls and the surrounding were checked using nine thermocouples. Before the measurements where performed the cavity was left in the dark with the baths switched on for at least six hours. This was done to ensure a steady state flow condition and a minimum of influence from outside light.

The coolant water for the laser was set at a temperature of 25.9 degree Celsius with a flow rate of 2.3 $\pm$ 0.1 L/min. The power output of the laser was set at 1.5 Watt. From the scope this resulted in the power outputs as listed below in Table 3.1. The alignment of the Fiberlight and its connecting optics are weekly optimized, so these value may vary a little bit in time. For a perfectly functioning setup, the power outputs should be about the same for each output canal. A difference in intensity between the green and blue light is normal, but the power outputs from the unshifted and shifted channels should be equal. Since the system is carefully aligned every week, it can be concluded that the measurement equipment is not in optimal condition. More information on the condition of the equipment and the related consequences is given in Section 4. The vertical velocity was measured using the green bundles which were able of capturing the highest data rate. The blue bundles were not capable of capturing the horizontal velocities which are much lower compared to the vertical velocities. Therefore only measurements of the vertical velocity were recorded. The bundles leave the scope under an angle of 3.95 degree [35]. To be able to measure close to the wall without the laser bundles being blocked, the scope was positioned under an angle of 5 degree towards the wall. When processing measurement data of horizontal velocities, this should be accounted for.

The light scattered by the particles is captured by the scope and filtered to get rid of noise. First a filter which only allowed the frequency band of 0.3 - 3 kHz was used with a downmix frequency of 39.9997 MHz used. This was not sufficient since all negative velocities were filtered out of the signal. The new set of measurements was filtered using a frequency band of 1 - 10 kHz with a downmix frequency of 39.9945 MHz.
Two types of measurement grids were used, one according to the specifications of Popin-

Table 3.1: Averaged power outputs from the scope

output canal	averaged power [mW]
green unshifted	68
green shifted	9
blue unshifted	9
blue shifted	5

hak; 59 points from one wall to the middle of the cavity. The first three points were at a distance 0.25, 0.38 and 0.50 mm from the wall. Between 0.50 and 2.00 instances of 0.25 mm were used. Between 2.00 and 15.50 every 0.50 mm and from 15.50 instances of 1.00 mm were used [3]. This sequence was performed at different heights at both sides of the cavity. Each position was measured for eight minutes or 600 data entries.
The second measurement grid was less fine due to time limitations; it featured 13 points, starting close to the cavity walls with a distance of 1 mm between each point. Measurements were performed for two minutes or 111 data entries. The validity of these results from measurements with fewer data entries will be explored in Sections 4.2 and 5.2.

The captured velocity data was exported and evaluated using MATLAB. Averaged values of the velocities were calculated and plotted, as well as the average velocity per number of measurements. The latter was done to obtain insight in the minimum amount of data entries required to get reliable results.

3.3 Measurement of confined fluids

The laser light from the LDV probe travels through different media, which results in the refraction of the light. This changes the position of the measured volume. The angle at which the light is refracted is described using Snell's law, which gives a relation between the refractive indices and the incident and refractive angle for the adjacent media [37]. Snell's law is given by Equation 3.1.

$$n_1 \sin\theta_1 = n_2 \sin\theta_2 \tag{3.1}$$

Here n denotes the refractive index of the material. In the measurement setup utilized in this research, the laser first has to cross three different types of media. First through the air, then the acrylic wall of the cavity and finally through the water inside the cavity. For this system with three different media Snell's law from Equation 3.1 becomes

$$n_a \sin\theta_a = n_g \sin\theta_g = n_w \sin\theta_w \tag{3.2}$$

In Equation 3.2, the subscript a, g and w stand for air, glass (acrylic) and water respectively. The angle at which the laser beams leave the probe θ_a is given to be 3.95 degree [37]. The values for the indices of refraction used in this research are listed in Table 3.2 and are taken from different books on this subject as cited in [32, 38].

Table 3.2: Overview of the different refractive indices [32, 38].

medium	refractive index n_i
air	1.000
water	1.333
acrylic glass	1.491

Equation 3.3 relates the position of the probe to the location of the measurement volume and is adopted from Equation 14.27 of Albrecht's Laser Doppler and Phase Doppler Measurement Techniques as cited in [32].

$$y_w - y_a = y_a \left(\frac{n_w}{n_a} - 1 \right) + t \left(1 - \frac{n_w}{n_g} \right) \tag{3.3}$$

In this equation y_w and y_a respectively denote the position of the measurement volume and the probe, whereas t denotes the thickness of the acrylic wall. To find the displacement of the measurement volume with respect to the displacement of the probe, Equation 3.3 is differentiated with respect to y_a resulting in Equation 3.4.

$$\frac{dy_w}{dy_a} = \frac{n_w}{n_a} = n_w \tag{3.4}$$

From Equation 3.4 it can be seen that the movement of the measurement volume is related to the movement of the probe via a factor equal to the refraction index of the water, which is equal to 1.333. For example to move 10 mm inside the cavity, the probe only has to travel $10/1.333 = 7.502$ mm.

Chapter 4

Results

The reliability of results obtained by measurements is strongly dependent on the performance of the equipment used. Unfortunately the LDV equipment used in this research gave a lot of problems in terms of performance. The number of subsequent measurements that could be conducted was limited due to a malfunctioning Bragg cell power supply unit. This was unable to amplify the 40 MHz shifted beams leaving the Bragg cell enough to match the required intensity of the unshifted beams, as is shown in Table 3.1. Apart from that, the main problem was that it could not power the Bragg cell for longer periods of time. Therefore only measurements could be conducted for short periods of time in the order of a couple of hours. After this it needed to be switched off for at least an equal amount of time before the measurements could be continued. To give an idea of the limitation this imposed; Popinhak measured the flow profile in the cavity at nine different heights, each height consisting out of 128 points. Every point was measured for eight minutes. Redoing all of his measurements would take 135 hours of doing non-stop measurements. It was simply impossible to exactly redo his measurements. Therefore it was chosen to measure on a courser grid and also to measure every point only for two minutes or 111 successful particle detections. To guarantee the accuracy of the results, the measurement data is analysed to find a minimum of particle detections necessary.

What became clear after the visit of a specialized external technician was that the optic fibres connecting the beam shifter to the scope were in a very bad condition. In a system in good condition about 60% of the power generated by the laser is lost in the transmitting optics. In our LDV setup about 94% is lost. This can not be solved by increasing the power output of the laser, since also the quality of the laser beam is of influence on the results. A high quality laser beam will create a well defined (neat) measurement area. When a large part of the signal is lost during transmission, the measurement area will be of lesser quality. This will result in a lower data rate and reliability of the results

4.1 Number of particles in the cavity

In previous work there was no notion given regarding the exact amount of particles in the cavity required to do measurements. What was learned from previous executors of the experiment, was that they used to mix about half a teaspoon of particles with the water in the cavity. This was copied by us in our first experiments, resulting in a zero data rate from the cavity. Since there was data when a wider frequency filter band was reviewed, the calculations used to choose the filter and frequency shift were double checked. When these seemed all correct, it was concluded that the problem must be in the cavity itself, specifically in the amount of particles in the cavity flow.
Since there was no signal captured from the cavity, the first conclusion was that the number of particles had to be to low, so it was increased. The original amount of particles added (half a teaspoon) was weighted and increased. Later also the data rate was tested for lower amounts of particles, denoted *small* in Table 4.1. These initial experiments (the first four entries of Table 4.1) gave no clear results on the correct required amount of particles.
An overview of all the different variations used is given in Table 4.1. Limited by the accuracy of the scale initially used, for the majority of the tests it was only possible to do rough estimations of the added amount of particles. This accounts for the first five entries of Table 4.1.

Table 4.1: Overview of the different amounts of particles used in the cavity in order to obtain data readings.

amount by visual inspection	weight [gram]	data rate present
normal; half a teaspoon	0.2 ± 0.01	sometimes
very large	± 0.8	no data rate
small	± 0.1	no data rate
small	± 0.05	no data rate
very small	0.005 ± 0.0025	steady data rate
very small	0.0068	steady data rate

When the initial experiments gave no useful results, more information on the topic of correct amount of seeding particles was found in the PDPA/LDV operations manual. In the manual is stated that the optimal particle density is one particle per measurement volume [5]. The measurement volume is given in Equation 4.1 which is adopted from Equation 5.41 from Albrecht's Laser Doppler and Phase Doppler Measurement Techniques as cited in [32].

$$V_0 = \frac{8\pi}{3} \frac{r_w^3}{\sin\theta} \tag{4.1}$$

In this equation r_w is the radius of the laser beam waist and θ is the angle under which the intersecting laser beams cross each other [32]. Filling in these values, which were found in the FlowSizer software results in a measurement volume of 4.39×10^{-2} mm^3 for the intersecting green bundles and 3.75×10^{-2} mm^3 for the blue bundles.

As described in the PDPA/LDV operations manual, the optimal particle density is equal to the inverse of the measurement volume [5]. The particles are assumed to be spherical and have a radius of 0.25 μm. Using this, the volume of one particle can be calculated. Combined with the known volume of the cavity and particle mass (1.03 kg/dm^3), the required total particle mass for the cavity was calculated to be 0.0072 gram, based on the measurement volume created by the blue laser bundles and 0.0061 gram for the green measurement volume.

Indeed measurements performed with an added particle mass of 0.005 $\pm$0.0025 gram did result in a constant data rate. The uncertainty of this number is based on resolution of the scale used resolution, which is 0.01 gram. The procedure to obtain the stated amount of particles consisted out of measuring 0.01 gram and adding half of the amount to the cavity. When more accurate weight measurements where possible, experiments were conducted with a well defined 0.0068 gram of particles. This showed very good results in terms of data rate.

4.2 Number of data readings

An important parameter in terms of efficiency is the number of data readings from particles passing through the measurement volume required to obtain a reliable averaged velocity. This was studied by doing measurements for a longer period of time at the same position and calculating the average velocity per number of measurements. The data used to create the velocity profiles in Section 4.3 is analysed in the same way to ensure that reliable results are presented there.

Shown in Figure 4.1 is the typical behaviour of the averaged value of the vertical velocity per number of data measurements at a certain position. The two horizontal lines indicate the boundaries of the rounded average over the total set of velocity data.
The convergence of the averaged value of the velocity near the cold wall at 0.7 cavity height is shown in Fig. 4.2. The data used to create this graph is also used to create the velocity profile near the cold wall in Figure 4.3c. The velocities are averaged after x number of measurements and rounded to the order of 0.1 mm/s. Note that the absolute rounded velocities are shifted in this graph. Of importance here is the change in rounded velocity with increasing number of data counts.

4.3 Velocity profiles

Velocity measurements were performed near the hot and the cold wall at different heights as described in Section 3.2. The first set of measurements was performed on the same fine grid as Popinhak used, however using incorrect filter and downmixing settings. This resulted in only positive velocity measurements, since the negative measurements were filtered from the signal. Measurements with the correct settings were due to time limitations performed on a less fine grid with a spacing of 1 mm. The maximum data count was set

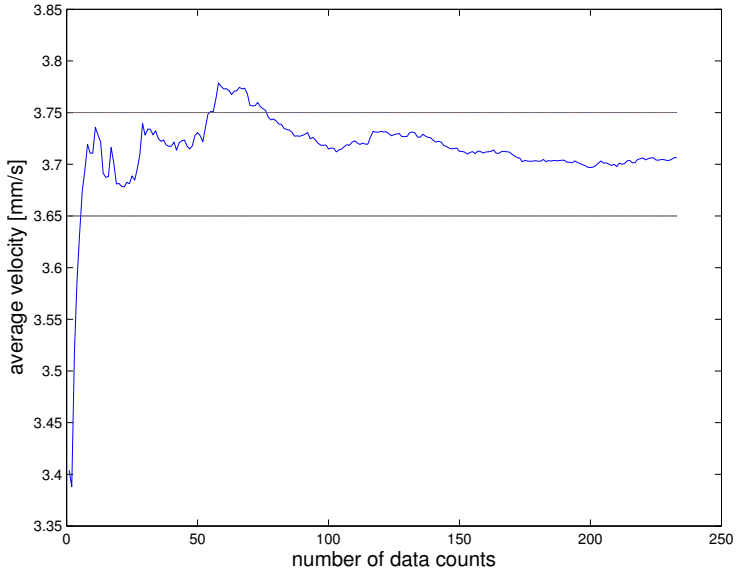

Figure 4.1: The averaged value of the vertical velocity per number of data measurements and the boundaries of the rounded average velocity.

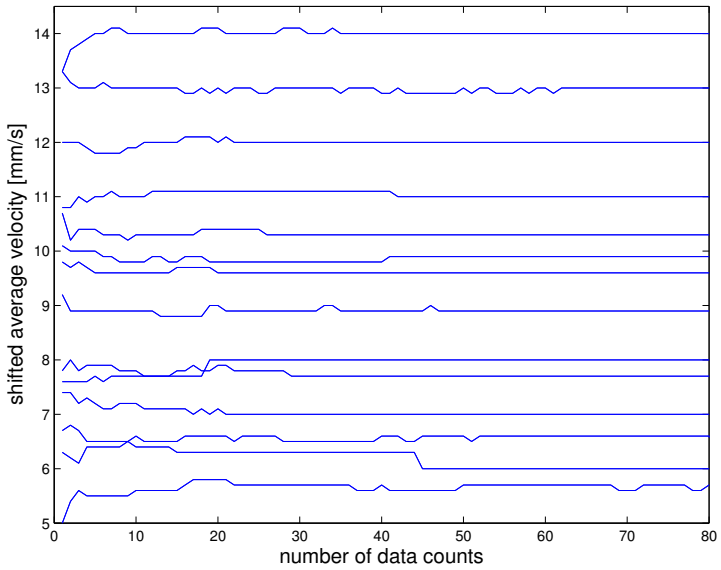

Figure 4.2: Shifted rounded average velocities near the cold wall at 0.7 cavity height.

at 111 or two minutes of measurements per measurement location for reasons explained in Section 5.2.

Shown below in Figure 4.3 are the velocity profiles from the measurements near the hot and the cold wall for a cavity height of 0.3 and 0.7 times the total height. Also the results

for the cold wall are shown at a height of 0.5 cavity height. The measurement results near the hot wall at 0.5 cavity height are missing due to time limitations. Priority was given to measurements near the cold wall, in order to be able to make a statement regarding the cold wall results from Popinhak. The heights are expressed as fractions of the total cavity height; 0.1 cavity height would correspond to 40 mm from the bottom, 0.2 cavity height to 80 mm from the bottom and so on.

Note that a distance of 0 mm from the wall in Figure 4.3 should be interpreted as very close to the wall. The other positions on the x-axis indicate the distance to this point. At the wall itself the flow velocity can be assumed zero in accordance to the no slip condition boundary condition.

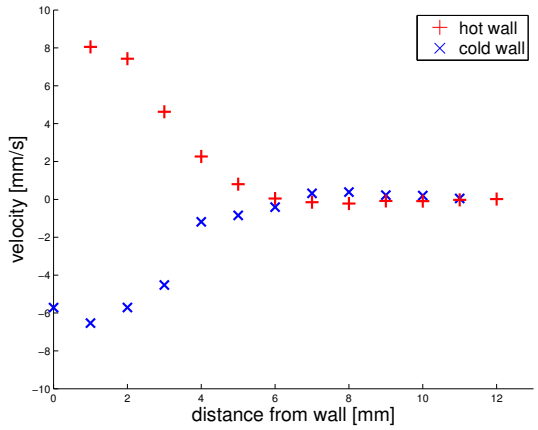

(a) 0.3 cavity height

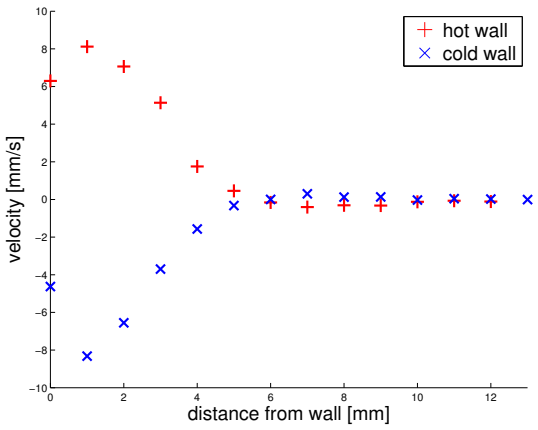

(b) 0.7 cavity height

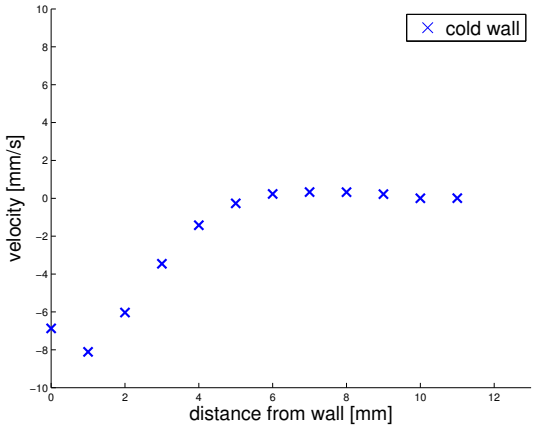

(c) 0.5 cavity height

Figure 4.3: Measurement results at 0.3, 0.5 and 0.7 cavity height.

Chapter 5

Conclusions and discussion

The goals for this internship were to perform maintenance to get the setup back in operational condition, to redo the measurements performed by Popinhak and try to find an explanation for his somewhat anomalous results. The maintenance required a lot of time since the measurement equipment turned out to be in a lesser state than expected. Therefore the number of measurements that could be conducted was limited. Nevertheless some important conclusions can be drawn from the results.

5.1 Number of particles in the cavity

Based on the experimental results presented in Table 4.1, it is concluded that the amount of added polystyrene seeding particles in the flow is an important parameter in obtaining reliable results. The correct amount was calculated assuming that ideally at all times only one particle is present in the measurement volume. For the measurement volume created by the intersecting green laser bundles this was calculated to be 0.0061 gram of particles. For the blue bundles this is 0.0072 gram. Indeed experiments with a added amount of 0.0068 gram particles showed a steady data rate.

The question that rises based on these results is why Popinhak did find a (high) data rate, whilst it can be safely assumed that he used a particle density much higher than is calculated as being the optimum. In the master's thesis written by Popinhak (as cited in [3]) no mention is given of the amount of particles added to the cavity. Only after consultation with one of his temporary co-workers (Chris Willemsen) it was found that he used about half a teaspoon of particles. Clearly, the amount of particles was not found to be of influence at that time. One possible explanation for this is that the LDV measurement equipment was in a better condition at the time when Popinhak performed his measurements. Therefore the amount of particles might have been of lesser importance and the equipment was better capable of handling more particles in the measurement volume at the same time.

What also should be taken into account is that when larger amounts of particles are used,

not all the particles dissolve in the water. Large amounts of particles are seen to stick to the front, back and top walls of the cavity. This means that actually lower amounts of particles are dissolved than is being stated or assumed. This is also something to keep in mind when adding the calculated very low amounts of particles, since there will always be some particles that are not dissolved.

5.2 Number of data readings

From Figure 4.1 can be seen that after a small number of measurements, the averaged velocity is already close to the final averaged velocity within a range of 0.1 mm/s. Based on these results it is concluded that the average value after 100 measurements is accurate enough to be used in a velocity flow profile. To be on the safe side, a maximum number of 111 data measurements per measurement position is used in the experiments. In order to obtain insight in the flow profile, an error value of 0.1 mm/s is tolerated in this report. Based on Figure 4.1 the error will be smaller than 0.1 mm/s after 100 measurements. Thereby Figure 4.2 shows stable convergence which leads to the conclusion that the number of measurements chosen is sufficient and the results are reliable.

5.3 Velocity profiles

Although the measurements were not performed on a very fine grid, nor with the highest possible accuracy, some important conclusions can be drawn. The most important conclusion is that the flow profiles near the hot and cold wall look very symmetric. This includes the small backflow (sign change of velocity) when moving further from the wall.
The velocity profiles found in this research show near resemblance to the results from the numerical work by Trias et al. [2]. This is mainly seen in the symmetry between the flow profiles near the hot and the cold wall that can also be seen in Figure 2.3, which is adopted from the work by Trias et al.. Thereby, the backflow observed in Figure 4.3 is also reported near both the hot and cold wall side by Trias et al. [2]. The vortices in the time averaged flow as described by Trias et al. in the top and bottom corner of the hot, respectively cold wall are however not observed in this research [2]. Perhaps when a finer grid is used combined with measurements of the horizontal velocities it is possible to make a statement regarding this.

Saury et al. performed measurements for different Rayleigh numbers [4]. In contrary to their results we did find a backflow at the cold wall side, whereas Saury et al. only found this phenomena at the hot wall side [4]. The Rayleigh numbers used by Saury et al. are higher than the one used in this research (4.0×10^{10} - 1.2×10^{11} versus 1.14×10^{10}), but it is unlikely that this is causing the difference in results. Apart from this, no other significant differences are found when comparing the results from Saury et al. with the results presented in Section 4.3.

A lot of similarities are present between the results from different authors pointed out in this section and the results presented in Section 4.3. Therefore it is concluded that the measurements were performed accurately enough and the results are valid to draw conclusions from.

The most important motive for the research presented here, was to obtain better insight in the results found by Popinhak using the same cavity [3]. The literature research showed some similarities in terms of the secondary rotary flows found by Popinhak in the top and bottom corners of the hot, respectively cold wall. His results seem to be in accordance with the corner vortices found in the numerical study by Trias et al. [2]. The same goes for Popinhak's flow profiles near the hot wall. These show resemblances to the profiles found by both Trias et al. (as cited in [2]) and Saury et al. [4]. Important characteristics such as the shape of the flow profile and the relative size of the backflow match closely when they are compared.

A lot of confusion existed however regarding the flow profiles near the cold wall as found by Popinhak. These feature an almost sinusoidal velocity distribution due to an unproportionally large backflow. Also the maximum absolute velocities found near the cold wall are much lower than would be expected. These kind of results were not found in the literature study and also did not show up in the experimental work presented in this report.
One major difference in how the experiments were conducted by Popinhak was in the number of particles being added to the water in the cavity. This can however be disregarded as being the cause of the peculiar flow profile found near the cold wall, since this should also have influenced the flow or measurements near the hot wall.

Careful inspection of the settings files as used by Popinhak to perform his measurements revealed that he made a questionable choice when selecting the frequency filter and downmixing frequency. In the vast majority of his measurements, a frequency filter ranging from 0.3 to 3.0 kHz with a downmix value of 39.999 MHz was programmed. Using Eq. 2.18, the Doppler frequency $f_{doppler}$ can be determined as shown in Equation 5.1.

$$f_{doppler} = f_{filter} + f_{downmix} - f_{shift} \tag{5.1}$$

Filling in for the filter and downmix frequency (Popinhak used 0.3 - 3 kHz and 39.999 MHz) as well as the frequency of the Bragg cell used (40 MHz), the range of $f_{doppler}$ is found to be between -0.7 and 2 kHz. Using Eq. 2.17 this results in a velocity range between -2.6 and 7.5 mm/s for the green laser light and between -2.5 and 7.1 mm/s for the blue laser. What can be concluded from this is that Popinhak never was able to find a correct vertical flow profile near the cold wall, since the negative velocities below -2.6 mm/s were filtered from his results.

Although regarding this, it is still very strange that his velocity profiles displays the sinusoidal behaviour close to the cold wall. More sense would make a normal velocity profile being cut off at -2.6 mm/s, resulting in some sort of a negative plateau shape. Thereby,

the measurement from Popinhak at 0.9 cavity height, as shown in Figure A.1i, shows a maximum negative velocity of -3 mm/s at the cold wall side. Theoretically, with the above specified filter and downmixing frequency, the system should be unable to capture this.

Popinhak gives no information or motivation on the settings used for the filter and downmixing in his thesis [3]. Therefore, based on the abnormal velocity profiles and the argumentation given here, his results in the form of observations, flow profiles and conclusions based on LDV measurements near the cold wall side can be regarded as incorrect.

The flow profiles from Popinhak near the hot wall do not show any kind of peculiar behaviour and do fit within the filter and downmixing used. Therefore it is believed that these results are reliable. Apart from the LDV measurements, Popinhak also performed measurements using PIV (Particle Image Velocimetry). No research has been conducted to get more insight in the PIV results from Popinhak, so no statements can be made regarding these measurements, results or conclusions drawn based on this.

5.4 Recommendations for further research

Complete flow profile It would be good to have a complete overview of the flow profile at different heights in the cavity. This should contain the horizontal flow velocities as well. Using this data, a more quantitative analysis can me made of the results obtained by Popinhak. This would make it as well possible to further comment on the efficiency of the measurements; is the accuracy indeed assured when less data is used to calculate the averaged velocity. In order to obtain these results, measurements on a more refined grid have been prepared. These measurements can be carried out by the three bachelor students working in the same lab. Based on their results, an analysis can be made of which areas in the cavity display interesting flow features. Near the vicinity of these areas more measurements can be conducted on an even finer grid.

Change Rayleigh number A new set of measurements can be relatively easy obtained by changing the Rayleigh number. The Rayleigh number is directly related to the temperature difference between the hot and the cold wall. For instance temperature differences of 8.8 degree Celsius and 26.4 degree Celsius match the Rayleigh numbers of 1×10^{10} and 3×10^{10} as used in the numerical study by Trias et al. [2, 14]. Using these temperature differences it might be able to check the results by Trias et al., who showed that the point at which the boundary layer separates moves upstream with increasing Rayleigh number [2]. This can be seen in Figure 2.3, which is adopted from the work by Trias et al. as cited in [2].

Detection of vorticity To get more out of the obtained data, the standard deviation of the velocity measurements at a single position should be studied, to find if a connection exists with the vorticity at that position. In this research only time averaged flows

are studied, but with this connection it is also possible to make some comments on the instantaneous velocity field using the same datasets.

5.5 Recommendations for the lab

Maintenance of measurement equipment As servicing showed, the LDV equipment (beam separator, optic cables, couplers and scope) is in need of some extensive maintenance and calibration. Advised by the service engineer was to send everything back to the manufacturer in order to take care of all shortcomings. This would probably be expensive and since it is possible to perform, although limited, measurements with the equipment, the advice of minimal required action is to replace the Bragg cell amplifier for reasons explained in Section 4. The amplifier has been replaced before, probably somewhere in 2012, judging on the inscription on an old amplifier found in the lab. This would require contacting TSI (the manufacturer), since it is very difficult to find specifications or resellers for the Bragg cell amplifier. The visiting service engineer had no knowledge of whatsoever on the specifications of this amplifier. When contact is established with TSI, information can be exchanged on the efficiencies of the transmitting optics. Based on this information TSI will probably give an advice as well.

Electrical sockets The multiphase plug powering the laser is positioned directly under the return faucet for the cooling water. The first time the cooler was switched on after a long period of rest the connection was leaking. This was repaired, but it is strongly advised to review the possible dangers caused by this arrangement.

Acknowledgements

It is both challenging and exciting to find and work on an internship abroad. Apart from the practical matters, there are also cultural differences to overcome. Luckily, there are always people who are willing to make life more easy.

First of all I would like to thank professor Harry Hoeijmakers from the University of Twente. He supported my worldly adventures and used his network of contacts to find me an assignment in Brazil. My professor in Brazil who I would like to thank is professor Cesar Deschamps. During my first few weeks he helped me to get settled and made sure I received help from Nara Santos in managing Brazil's bureaucracy. I am also very grateful for the faith and freedom he gave me in organizing my work in the lab. Every time I came for help or with new ideas, professor Deschamps took this very serious, which is something I really appreciate. He explained this to me as resulting from having such good experiences with other students from the University of Twente.

The three students working with me were Heitor Paes de Andrade, Domicio Moura Lopes and Marcelo Ruaro Bortoli. Apart from helping me with my work, they also made that I had a great time working in the lab. After three months we said goodbye as friends and I hope to meet them again some day.

My brother Jan-Willem Bullee helped me with editing this report. His critical notes on both my writing and the form of the report were of great help in creating this final version.

Bibliography

[1] S. Xin and P Le Quéré. Direct numerical simulations of two-dimensional chaotic natural convection in a differentially heated cavity of aspect ratio 4. *Journal of Fluid Mechanics*, 304:87–118, 1995.

[2] F. X. Trias, A. Gorobets, M. Soria, and A. Oliva. Direct numerical simulation of a differentially heated cavity of aspect ratio 4 with Rayleigh numbers up to 10×10^{11} Part I: Numerical methods and time-averaged flow. *International Journal of Heat and Mass Transfer*, 53(4):665–673, January 2010.

[3] A. R. Popinhak. Investigação experimental da convecção natural terbulenta em uma cavidade com paredes verticais a diferentes temperaturas e razão de aspecto 4. Master's thesis, Universidade Federal de Santa Catarina, 2013.

[4] D. Saury, N. Rouger, F. Djanna, and F. Penot. Natural convection in an air-filled cavity: Experimental results at large Rayleigh numbers. *International Communications in Heat and Mass Transfer*, 38(6):679–687, 2011.

[5] *Phase Doppler Particle Analyser (PDPA) / Laser Doppler Velocimeter (LDV).* TSI Incorporated, revision d edition, 2005.

[6] Y. A. Çengel. *Heat Transfer: A Practical Approach.*

[7] F. P. Incropera and T. L. Bergman. *Fundamentals of Heat and Mass Transfer.* 2011.

[8] Turbulent natural convection of air in a non-partitioned or partitioned cavity with differentially heated vertical and conducting horizontal walls. *Experimental Thermal and Fluid Science*, (29):137 – 157, 2009.

[9] H. Benard. *Les Tourbillons cellulaires dans une nappe liquide transportant de la chaleur par convection en régime permanent.* PhD thesis, 1901.

[10] P. K. Kundu, I. M. Cohen, and D. R. Dowling. *Fluid Mechanics.* 5 edition, 2012.

[11] The Engineering Toolbox, http://www.engineeringtoolbox.com, visited 12-03-2014.

[12] UCLA Hall of Pioneers, http://www.seas.ucla.edu/jht/pioneers/pioneers.html, visited 21-03-2014.

[13] J. Holman. *Heat Transfer*. 2009.

[14] F. X. Trias, A. Gorobets, M. Soria, and A. Oliva. Direct numerical simulation of a differentially heated cavity of aspect ratio 4 with Rayleigh numbers up to Part II: Heat transfer and flow dynamics. *International Journal of Heat and Mass Transfer*, 53(4):674–683, 2010.

[15] R. B. Bird, W. E. Stewart, and E. N. Lightfoot. *Transport Phenomena, Revised 2nd Edition*. 2nd edition, 2006.

[16] T. L. Lee and T. F. Lin. Transient three-dimensional convection of air in a differentially heated rotating cubic cavity. *International Journal of Heat and Mass Transfer*, 39(6):1243–1255, 1996.

[17] W. H. Leong, K. G. T. Hollands, and A. P. Brunger. Experimental Nusselt numbers for a cubical-cavity benchmark problem in natural convection. *International Journal of Heat and Mass Transfer*, 42(11):1979–1989, 1999.

[18] Y. T. Ker and T. F. Lin. A combined numerical and experimental study of air convection in a differentially heated rotating cubic cavity. *International Journal of Heat and Mass Transfer*, 39(15):3193–3210, 1996.

[19] D. Dabiri. The Effects of Forced Boundary Conditions on Flow Within a Cubic Cavity Using Digital Particle Image Thermometry and Velocimetry (DPITV). *Experimental Thermal and Fluid Science*, 13:349–363, 1996.

[20] W. Schöpf and J. C. Patterson. Visualization of natural convection in a side-heated cavity: Transition to the final steady state. *International Journal of Heat and Mass Transfer*, 39(16):3497–3509, 1996.

[21] M. A. H. Mamun, W. H. Leong, K. G. T. Hollands, and D. A. Johnson. Cubical-cavity natural-convection benchmark experiments: an extension. *International Journal of Heat and Mass Transfer*, 46(19):3655–3660, 2003.

[22] W. Nusselt. *Die Wärmeleitfähigkeit von Wärmeisolierstoffen*. Mitteilungen über Forschungsarbeiten auf dem Gebiete des Ingenieurwesens. 1909.

[23] E. R. G. Eckert and W. O. Carlson. Natural convection in an air layer enclosed between two vertical plates with different temperatures. *International Journal of Heat and Mass Transfer*, 2:105–120, 1961.

[24] G. K. Batchelor. Heat Transfer by Free Convection across a Closed Cavity between Vertical Boundaries at Different Temperatures. *Quarterly of Applied Mathematics*, 12:209–233, 1954.

[25] F. Penot, A. N'Dame, and P. Le Quéré. Investigation of the route to turbulence in a vertical differentially heated cavity. *Proceedings of the 6th International Heat Transfer conference*, pages 417 – 422.

[26] F. Penot, O. Skurtys, and D. Saury. Preliminary experiments on the control of natural convection in differentially-heated cavities. *International Journal of Thermal Sciences*, 49(10):1911–1919, 2010.

[27] R. J. A. Janssen, R. A. W. M. Henkes, and C. J. Hoogendoorn. Transition to time-periodicity of a heated cavity. *International Journal of Heat and Mass Transfer*, 36 (11):2927–2940, 1993.

[28] R. J. A. Janssen and R. A. W. M. Henkes. Instabilities in three-dimensional differentially-heated cavities with adiabatic horizontal walls. *Physics of Fluids*, 8 (1), 1996.

[29] G. Labrosse, E. Tric, H. Khallouf, and M. Betrouni. A Direct (Pseudo-Spectral) Solver of the 2D/3D Stokes Problem: Transition To Unsteadiness of Natural-Convection Flow in a Differentially Heated Cubical Cavity. *Numerical Heat Transfer, Part B: Fundamentals*, 31(3):261–276, 1997.

[30] F. X. Trias, M. Soria, A. Oliva, and C. D. Pérez-Segarra. Direct numerical simulations of two- and three-dimensional turbulent natural convection flows in a differentially heated cavity of aspect ratio 4. *Journal of Fluid Mechanics*, 586:259–293, 2007.

[31] R. J. A. Janssen and R. A. W. M. Henkes. Influence of Prandtl number on instability mechanisms and transition in a differentially heated square cavity. *Journal of Fluid Mechanics*, 290:319–344, 1995.

[32] H. E. Albrecht, M. Borys, N. Damaschke, and C. Tropea. *Laser Doppler and Phase Doppler Measurement Techniques*. 2003.

[33] The Prospector Materials Database. Acrylic Typical Properties Generic Acrylic (PMMA), http://plastics.ides.com/generics/3/c/t/acrylic-properties-processing, visited 11-03-2014.

[34] TSI webinar notes cq powerpoint presentiation on LDV PDPA Optics, ftp://ftp.tsi.com/pub/fluid

[35] *TR/TM Series Fiberoptic Probes Manual*. TSI, Revision C edition, January 2007.

[36] TSI website, http://www.tsi.com/3-axis-traverse-system/, visited 23-04-2014.

[37] *TR/TM Series Fiberoptic Probes Owner's Manual*. TSI Incorporated, revision c edition, 2007.

[38] E. Hecht. *Optics*. 4th edition, 2003.

Appendix A

Measurement results by Popinhak

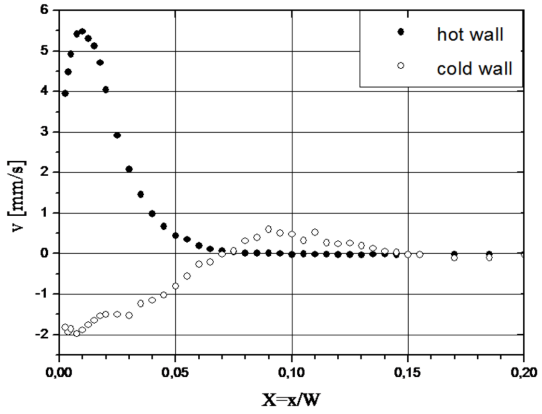

(a) 0.1 cavity height

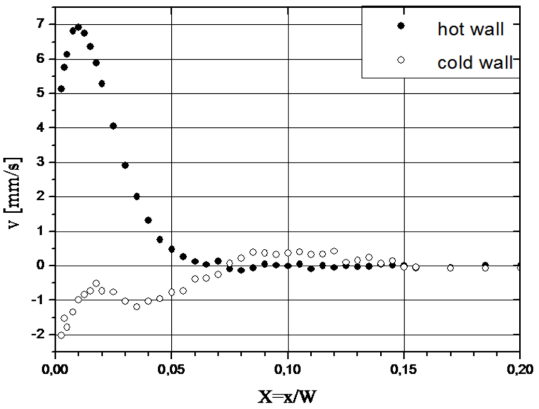

(b) 0.2 cavity height

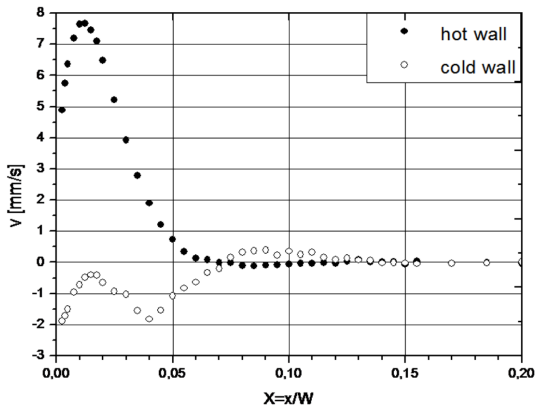

(c) 0.3 cavity height

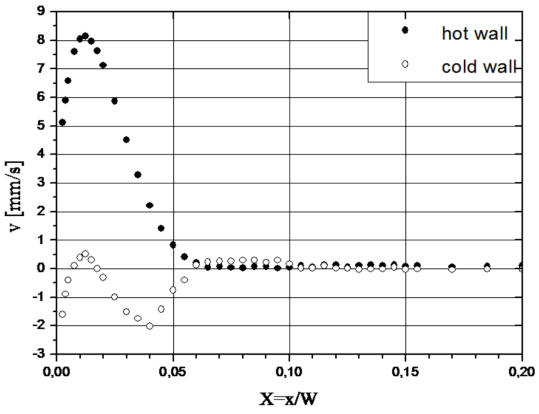

(d) 0.4 cavity height

Figure A.1: First part of the measurement results by Popinhak.

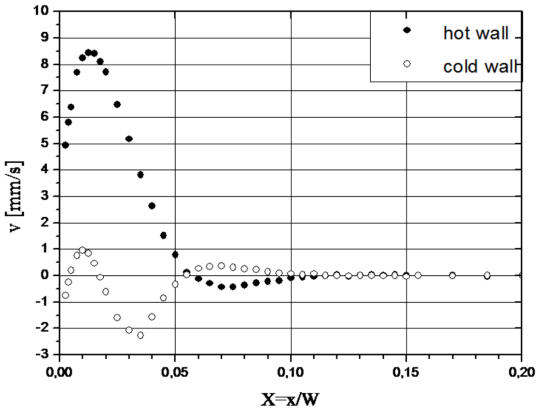

(e) 0.5 cavity height

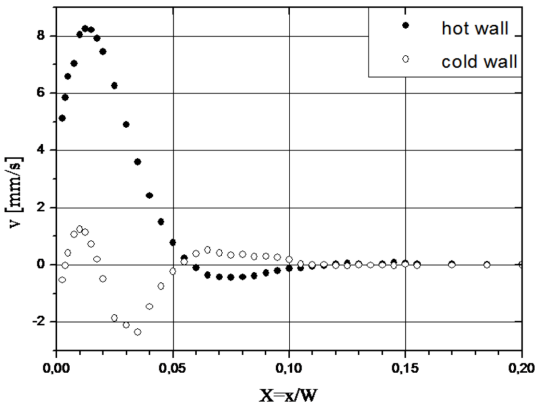

(f) 0.6 cavity height

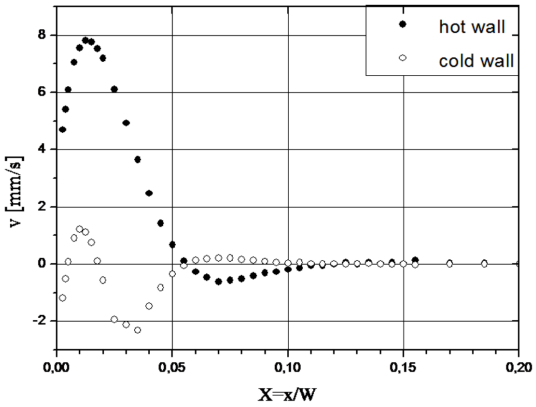

(g) 0.7 cavity height

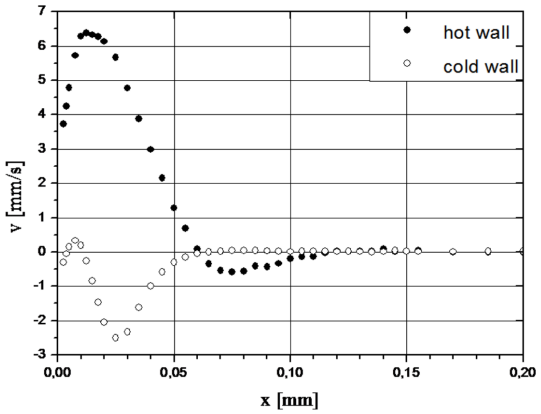

(h) 0.8 cavity height

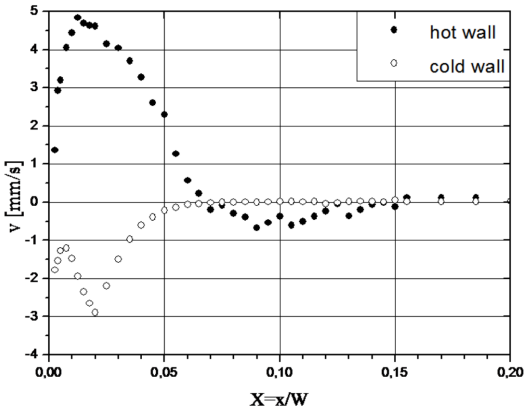

(i) 0.9 cavity height

Figure A.1: Second part of measurement results as presented by Popinhak in his master's thesis as cited in [3]. Plotted are the vertical flow velocities near both the hot and the cold wall as a function of the distance to the corresponding wall. Measurements where performed at different heights relative to the bottom of the cavity. The heights are expressed as fractions of the total cavity height; 0.1 cavity height corresponds to 40 mm from the bottom, 0.2 cavity height to 80 mm from the bottom and so on.